# Mechanically activated Piezo channels control outflow tract valve development through Yap1 and Klf2-Notch signaling axis

Anne Laure Duchemin[1,2,3,4], Hélène Vignes[1,2,3,4], and Julien Vermot[1,2,3,4]

[1]Institut de Génétique et de Biologie Moléculaire et Cellulaire, Illkirch, France

[2]Centre National de la Recherche Scientifique, UMR7104, Illkirch, France

[3]Institut National de la Santé et de la Recherche Médicale, U964, Illkirch, France

[4]Université de Strasbourg, Illkirch, France

## Abstract

**Mechanical forces are well known for modulating heart valve developmental programs. Yet, it is still unclear how genetic programs and mechanosensation interact during heart valve development. Here, we assessed the mechanosensitive pathways involved during zebrafish outflow tract (OFT) valve development *in vivo*. Our results show that the hippo effector Yap1, Klf2, and the Notch signaling pathway are all essential for OFT valve morphogenesis in response to mechanical forces, albeit active in different cell layers. Furthermore, we show that Piezo and TRP mechanosensitive channels are essential for regulating these pathways. In addition, live reporters reveal that piezo controls Klf2 and Notch activity in the endothelium and Yap1 expression in the smooth muscle progenitors to coordinate OFT valve morphogenesis. Together, this work identifies a unique morphogenetic program during OFT valve formation and places Piezo as a central modulator of the cell response to forces in this process.**

## Introduction

Heart pumping and shaping take place concomitantly during embryonic development. These two processes require a tight and dynamic coordination between mechanical forces and tissue morphogenesis. Heart valve development is a great model for studying these interactions when considering that heart valve defects are amongst the most common congenital cardiac malformation in human (Hoffman and Kaplan, 2002; Oyen et al., 2009). The multichambered heart contains two different sets of valves: arterial valves that are semilunar and mitral (atrioventricular) valves that are tricuspid. While the developmental programs driving mitral valve development are well established, less is known about arterial valves (Wu et al., 2017).

Congenital valve defects may originate from developmental origins and/or abnormal haemodynamic forces between these two sets of valves, and it remains unclear how general these developmental programs are. Aortic valves are located in areas of high flow velocity and mechanical forces have a great impact on valve morphogenesis (Butcher et al., 2008). Abnormal blood circulation is widely recognized as a cardiovascular risk factor and abnormal mechanotransduction has been associated with valvulopathies (Back et al., 2013). Congenital heart valve malformations are usually associated with genetic mutations in genes essential for heart valve development, such as signaling factors (Notch1, TGFβ) for the aortic valves (Back et al., 2013), and actin-binding proteins (FilaminA) for the mitral valves (Sauls et al., 2012). The constant discovery of genetic mutations linking valve defects with genes involved in controlling developmental programs (e.g., in NOTCH1, TBX5, GATA4, TBX20, LMCD1, TNS1, and DCHS1) (Dina et al., 2015; Durst et al., 2015; Garg et al., 2005; Richards and Garg, 2010), has spurred interest in valve morphogenesis. A key issue is to further define the genetic or environmental causes of valve malformation.

Abnormalities of the arterial valve leaflets are the commonest congenital malformations, in particular bicuspid aortic valve. Aortic valves mainly derive from endocardial cushion progenitors with a potential contribution from other cellular sources (epicardial cells and neural crest) (Wu et al., 2017). Generally, valve formation depends on two main events: cell proliferation, which is mainly mediated by the *vegf-nfat1* pathway, matrix deposition and an endothelial-to-mesenchymal transformation (endMT) under the control of Gata transcription factors (Laforest et al., 2011; Stefanovic et al., 2014), Notch signaling (Luxan et al., 2016), *Smad/tgf-beta/Bmp*, and *Wnt-beta catenin* signals (Combs, 2009). Nevertheless, recent evidences suggest that arterial valves develop differently from atrioventricular valve by differentiating directly from progenitors in the outflow wall independently from endMT (Eley et al., 2018).

The zebrafish constitutes a powerful model to study cardiac valve development and the role of mechanical forces at the cellular scale. Two sets of valves are formed in zebrafish: the outflow tract (OFT) and atrioventricular (AVC) valve. The cellular processes leading to valve formation are extremely dynamic and are particularly challenging to address *in vivo*. Zebrafish cardiac valve development is a great *in vivo* model to study valve development. Heart valves originate from progenitors located in the ventricle and atrium that generate the valve leaflets through a coordinated set of endocardial tissue movements (Boselli et al., 2017; Pestel et al., 2016; Steed et al., 2016a; Steed et al., 2016b; Vermot et al., 2009). The sequence of cellular events leading to AVC valve formation in zebrafish embryonic hearts is initiated through cell shape changes that lead to EC convergence towards the AVC (Boselli et al., 2017) and cellular rearrangements that will form a multilayered tissue (Beis et al., 2005; Pestel et al., 2016; Scherz et al., 2008; Steed et al., 2016b). In the zebrafish AVC, blood flow and Klf2a control *notch1b* and *bmp4* expression, both of which are necessary for valve formation (Vermot et al., 2009). Klf2a regulates the deposition of matrix protein (in particular Fibronectin1) in the valve forming area (Steed et al., 2016b), as well as Wnt signaling by controlling *wnt9b* expression (Goddard et al., 2017). The latter is consistent with the fact that canonical Wnt signals arise specifically in sub-endocardial, abluminal cells and that these Wnt signals are dependent upon hemodynamic forces in zebrafish (Pestel et al., 2016). In addition, Notch signaling is essential for aortic valve formation (Garg, 2016) and OFT development (MacGrogan et al., 2016; Wang et al., 2017). OFT valve development at the cellular and molecular scale, however, is largely unknown.

Fluid shear stress is an important environmental cue that governs vascular physiology and pathology (Baeyens et al., 2016), but the molecular mechanisms that mediate endocardial responses to flow are only partially understood. In zebrafish, the mechanosensitive channels Trpv4 and Trpp2 modulate endocardial calcium signaling and *klf2a* expression is necessary for valve morphogenesis and downstream pathway activation (Heckel et al., 2015; Steed et al., 2016b). Notch signaling is tightly involved in cellular mechanosensitive responses in human aortic valves (Godby et al., 2014) and Notch1 is a potent mechanosensor in adult arteries (Mack et al., 2017). More recently, it has been shown that stretch-sensitive channels from the Piezo family (Murthy et al., 2017) are important for vascular development (Li et al., 2014; Ranade et al., 2014) and lymphatic valve formation (Nonomura et al., 2018). In the embryo, Piezo channels exert essential roles during cell differentiation (He et al., 2018) and can affect lineage choice by modulating the nuclear localization of the mechanoreactive transcription coactivator Yap (Pathak et al., 2014). Nevertheless, the role of Piezo-mediated mechanotransduction during cardiac development and its potential targets remain unclear.

In the developing cardiovascular system, biomechanics is key for modulating flow propagation (Anton et al., 2013). In the teleost heart, the OFT constitutes a specialized organ comprising the bulbus arteriosus (BA). The BA acts as a windkessel by dampening the pressure wave down the arterial tree

(Braun et al., 2003b). To perform its function, the BA expresses elastic fiber genes that are thought to provide the mechanical properties necessary for its physiological function (Braun et al., 2003a, b; Keith et al., 1977). The BA is separated from the ventricle by the OFT valve and is composed of smooth muscle. The extracellular matrix (ECM) gene, elastin b, contributes to the development of the BA by regulating cell fate determination of cardiac precursor cells into smooth muscle via a process that involves the mechanotransducer Yap1 (Moriyama et al., 2016). How these factors contribute to OFT valve development and interact with other mechanosensitive pathways remains unclear.

In this study, we investigated the signaling events taking place during OFT valve formation and addressed their regulation by the mechanosensitive channels Piezo and TRP as well as the flow-responsive transcription factor Klf2a. We show that OFT valve formation proceeds via an initial stage of endothelial cell folding, which is associated with the generation of a cluster of smooth muscle cell progenitors surrounding the endothelial layer. Subsequent global tissue remodeling events result in the appearance of functional leaflets, which defines a unique process of valvulogenesis. Using live reporters to highlight the signaling changes accompanying these temporally coordinated cell-movement events and genetics, we identified Notch and Klf2 as key flow-dependent factors as well as YAP1 as necessary factors for the correct coordination of OFT valvulogenesis. We show that Piezo and Trp channels are key regulators of *klf2* activity in the endothelium and that piezo modulates yap1 expression in the smooth muscle cells, providing a molecular link between mechanosensitivity and cell signaling in the multi-tissular valve structure. These data describe the cell responses that are coordinated by the mechanical environment and mechanotransduction via mechanosensitive channels in the endothelium.

## Results

### Outflow tract valve morphogenesis is unique

In order to better understand the roles played by blood flow during outflow tract (OFT) valve development, we have developed imaging techniques to capture cardiac motion and analyze blood flow in the OFT. Live imaging of the double transgenic line *Tg(gata1:ds-red; kdrl:EGFP*) to follow red blood cells and endothelial cell wall movements reveal dramatic changes in intracardiac blood flow patterns during OFT valve development: as the heart matures, blood flow in the OFT is bidirectional until functional valve leaflets emerge in the OFT at 144 hpf (Figure 1 A-C). Throughout development, the periods within the cardiac cycle in which reversing flow can be observed decrease in length until 144 hpf, the stage at which we could not observe reversing flow anymore (Figure 1 C). Using the *Tg(fli:lifeact-EGFP; kdrl:nls-mCherry)* line, which labels endothelial cells, we found that these flow profile modifications are linked to changes in OFT tissue geometry and the state of OFT maturation (Figure 1 B). At 56 hpf, the endothelium resembles a tube (Figure 1 B, C), maturing into cushions by 72 hpf, into premature leaflets by 96 hpf and finally into elongated, thin leaflets by 144 hpf (Figure 1 B, C).

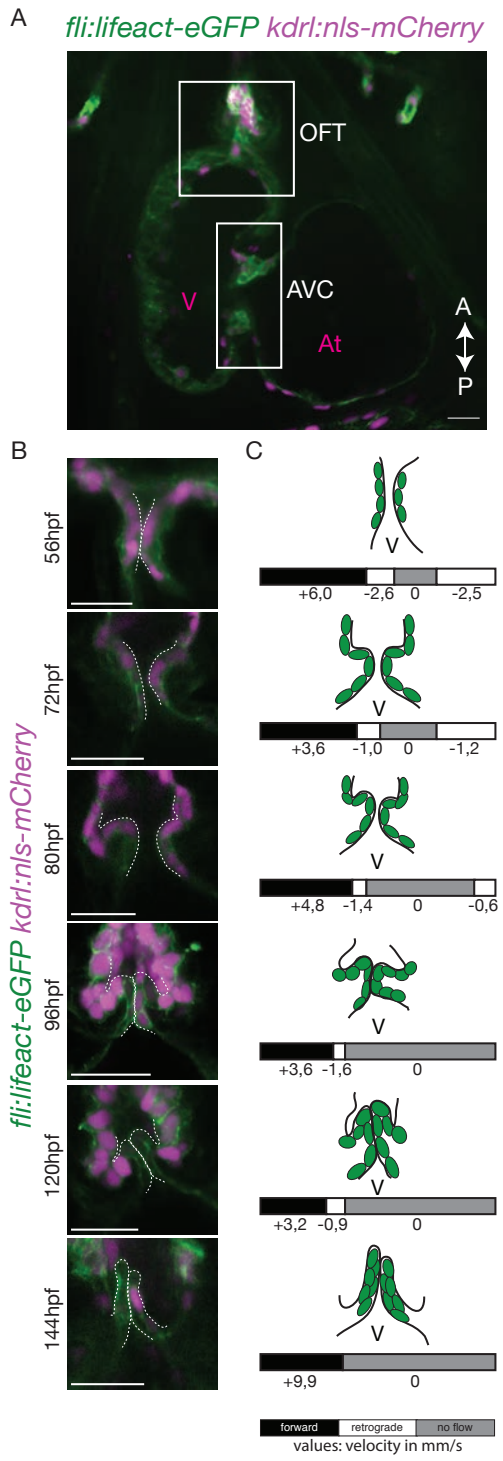


***Figure 1 – The OFT develops from 56 hpf to form functional valves at 144 hpf***

*(**A**) Z-section of the double transgenic line Tg(fli:lifeact-EGFP; kdrl:nls-mCherry) showing the overall structure of the heart. OFT: outflow tract, AVC: atrioventricular canal, At: atrium, V: ventricle. Scale bar: 20um. (**B**) Z-sections of the double transgenic line Tg(fli:lifeact-EGFP; kdrl:nls-mCherry) at different time-points showing the endocardial OFT structure. Scale bar: 25um. (**C**) Schematic representation summarizing the formation of the valve leaflets over time and flow profile in the OFT during development (from 56 hpf to 144 hpf) showing the forward flow (black), retrograde flow (white) and no flow (grey) fractions with the velocity of the red blood cells (in mm/s) using the double transgenic line Tg(gata1:ds-red; kdrl:EGFP). V: ventricle.*

To better characterize how the endothelium changes shape over time and how cells reorganize to form OFT valves, we performed photoconversion experiments using the *Tg (fli:gal4FF/UAS:kaede)* (Figure 2 A). We photoconverted Kaede from green to red in the cells located in the anterior, middle or posterior part of the valve at 72 hpf and assessed their position at 96 hpf and 120 hpf (Figure 2 A, B). The results suggest that the endothelium folds to form the valve without multilayering (Figure 1 B, C). Indeed, we could observe that the photoconverted cells remain attached to each other and do not show signs of delamination as observed in the AVC (Figure 2 B, C). Together, these results suggest that OFT valves form by a folding process that might involve the adjacent tissue.

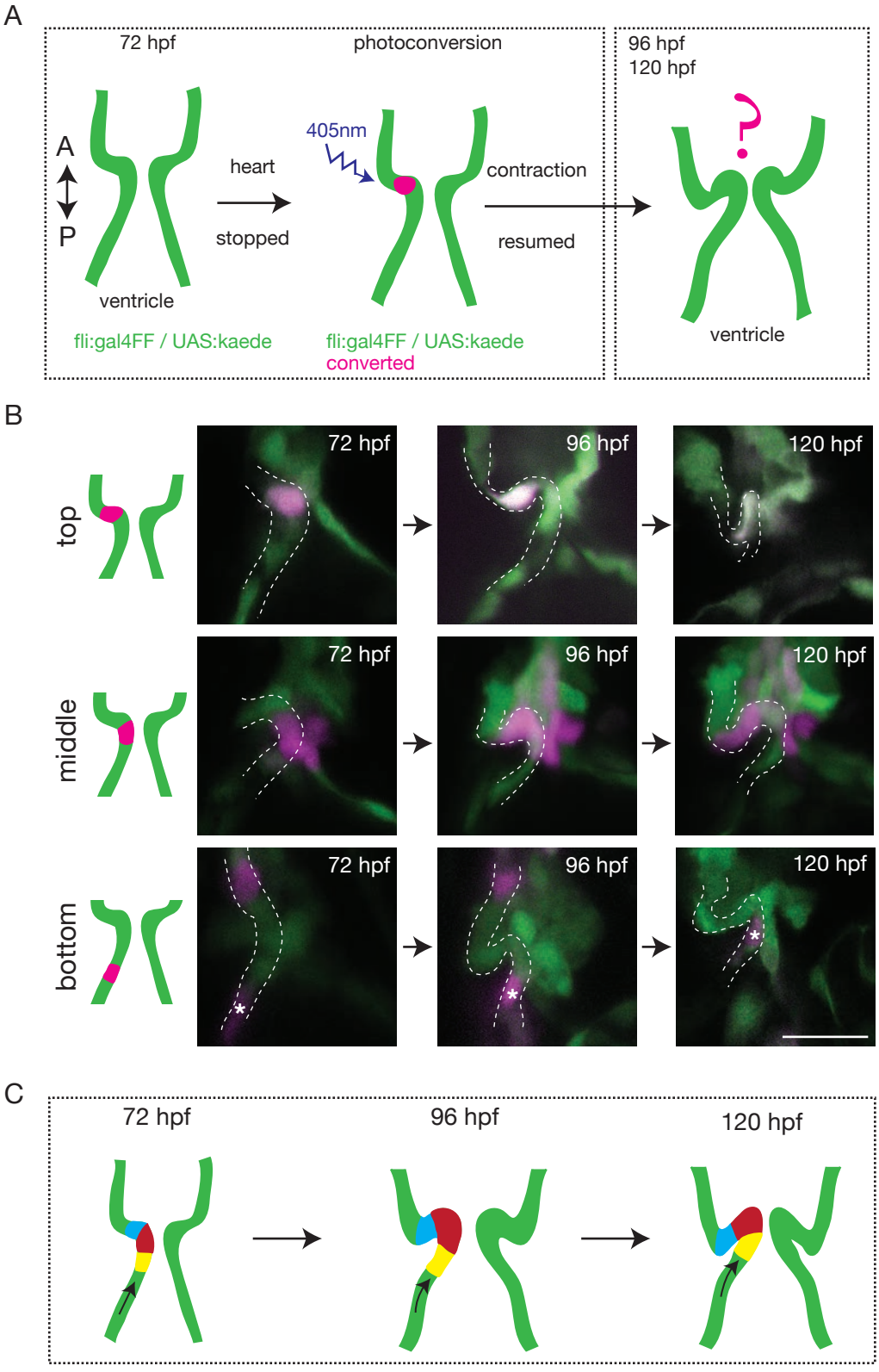


***Figure 2 – The endothelium contribution to emerging OFT valve leaflets***

*(**A**) Experimental set-up for the photoconversion studies. Heart was stopped at 72 hpf, the region of interest exposed to 405 nm light to convert kaede from green to red (shown in magenta) fluorescent form and heart contraction was resumed until 120 hpf. Beating hearts were imaged at 96 hpf and 120*

*hpf by spinning disk microscopy. A. Anterior, P. Posterior. (**B**) Z-sections of the Tg(fli:gal4FF/UAS:Kaede) line just after photoconversion (72 hpf), and at 96 hpf and 120 hpf. The star highlights the photoconverted cell in the top (n=6), middle (n=5) and bottom (n=4) part of the OFT valve. Scale bar: 20 um. (**C**) Schematic representation of the results of the photoconversion studies showing the folding of the endothelium in the OFT.*

The cellular contribution of the OFT valve led us to the hypothesis that the surrounding tissue could contribute to valve morphogenesis. We analyzed Fibronectin1 (Fn1) expression in the OFT by counterstaining the *Tg(kdrl:EGFP)* with the Fn1 antibody (Figure 3 A-D). We found that Fn1 deposition in the OFT is very different from that in the AVC (Steed et al., 2016). At 72 hpf, cushions appear and Fn1 is observed in the cells around the endothelial cells, that are themselves surrounded at their base by myocardium in the posterior part (Figure 3 A, A', A", B, B", C, C", D, D"). Fn1 expression level increases at 96 hpf and delineates a group of cells surrounding the OFT as well as in the basal side of a few endothelial cells that form the cushions (Figure 3 C, arrows, C"). In the developed leaflets at 120 hpf, Fn1 expression is maintained within the leaflets (Figure 3 D, D"). We found that the cells surrounding the OFT that strongly express Fn1 also express Elastin b (Elnb, Eln2 or Tropoelastin), a marker of smooth muscle cells (Paffett-Lugassy et al., 2017) (Figure 3 B', C', D'). We could confirm that the cells surrounding the Fn1 cells are not myocardial cells as the myocardium stops just before the OFT region (Figure 3 A, A'). Some of these cells also express *Tg(wt1a:GFP)* (asterisks in Figure 3 E) a marker of pericardial cells (Peralta et al., 2014), suggesting that they may have originated from pericardial precursors. Together, these results suggest a developmental sequence of OFT morphogenesis *in vivo* where endothelial cell reorganization is associated with changes in gene expression in the surrounding smooth muscle cell progenitors. This indicates that the OFT morphogenesis involves remodeling of not just the endocardium, but also of a group of smooth muscle cells that express Fn1. We conclude that the tissular remodeling occurring during OFT valve development is significantly different from AVC valve development where the endocardium is the main remodeling tissue (Beis et al., 2005; Pestel et al., 2016; Steed et al., 2016b).

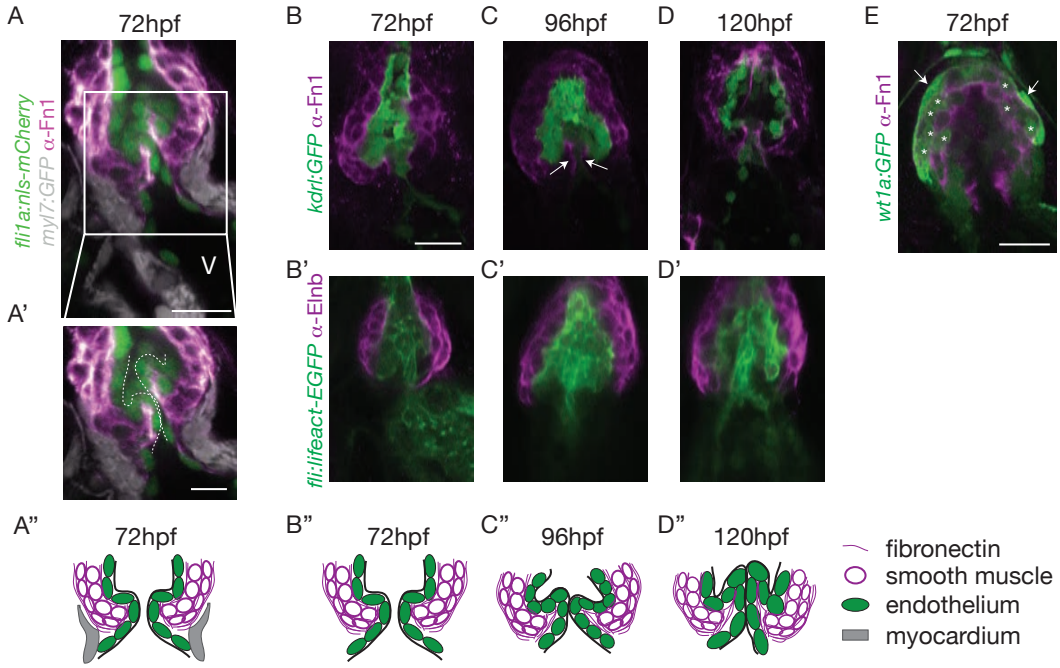


***Figure 3– The OFT endothelium is surrounded by smooth muscle cell progenitors expressing fibronectin and elastin***

*(**A**) Staining of Fibronectin1 (magenta) on Tg(myl7:GFP; fli1a:nls-mCherry), highlighting the myocardium (white) and the endothelium (green) at 72 hpf. Scale bar: 10 um. V : ventricle. (**A'**) Zoom of the OFT region in **A**. Scale bar: 10um. (**A"**) Scheme of the three layers shown in **A'** (magenta, smooth muscles; green, endothelium; grey, myocardium. Fibronectin1 (anti-Fn1, magenta) counterstaining on Tg(kdrl:GFP) and Elastinb (anti-Elnb, magenta) counterstaining on Tg(fli:lifeact-eGFP) showing their expressions in the OFT and scheme of the OFT at 72 hpf (**B**, **B'**, **B"** respectively) at 96 hpf (**C**, **C'**, **C"** respectively) and at 120 hpf (D, D', D" respectively). Scale bar: 20 um. (**E**) Co-localization of Fibronectin1 (magenta) with the Tg(wt1a:GFP) line at and 72 hpf. Scale bar: 20 um. Arrows show the epicardium and asterisks show the epicardium/Fn1 double positive cells.*

**Klf2, Notch signaling, and Hippo pathways are active in the OFT in different cell layers and are all necessary for proper OFT valve development**

To elucidate how these early events are regulated, we sought to determine the mechanosensitive signaling pathways activated at these early stages of OFT valve formation. We first assessed the activity of Klf2a reporter line (*Tg(klf2a:H2B-GFP)*) (Figure 4 A), which is a well described flow responsive reporter (Heckel et al., 2015; Steed et al., 2016b) and the Notch reporter *Tg(tp1:dGFP)* (Figure 4 B) which is well active in the progenitors of the AVC cardiac valves (Pestel et al., 2016). We could observe a specific activation of the Klf2a reporter in the OFT endothelium (Figure 4 A, C), in particular in the ventricular part of the valve (posterior) from 72 hpf to 120 hpf (Figure 4 C, D). Similarly, the Notch reporter *Tg(tp1:dGFP)* is specifically expressed in the OFT endothelium (Figure 4 B,C), in the ventricular part of the valve from 72 hpf to 120 hpf (Figure 4 C, D). Interestingly, the spatial activation of the reporter varies within the valve forming area - the transgene activation is stronger in the posterior part of the valve than the anterior part of the valve throughout the process of valve maturation (Figure 4 C, D). We made similar observations for the Notch reporter (Figure 4 C, D). These results suggest that

*klf2a* and Notch signaling are activated specifically in the part of the valve corresponding to where the OFT has the smallest diameter and where shear stress is expected to be the highest, consistent with the hypothesis that *klf2a* and Notch signaling are flow-responsive.

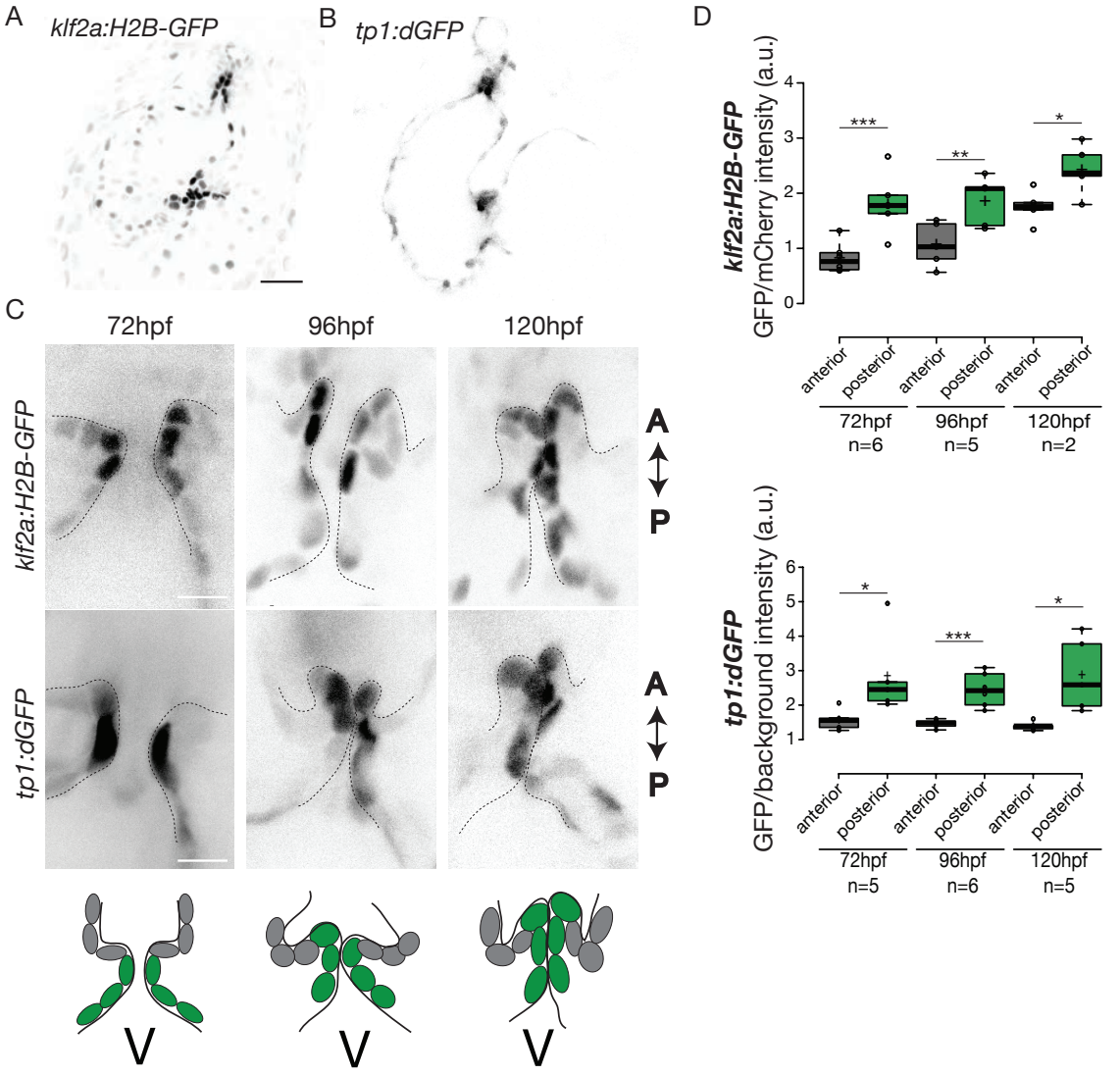


***Figure 4 – Klf2a and Notch reporters are activated in the OFT endothelium***

*Confocal z-section of the Tg(klf2a:H2B-GFP; fli:nls-mCherry) (**A**) and Tg(tp1:dGFP) (**B**). Scale bar: 20um. (**C**) Confocal z-section of OFT valves expressing the Klf2a reporter and Notch reporter at 72 hpf, 96 hpf, and 120 hpf. Schemes explaining the considered anterior (grey) and posterior (green) parts of the valve at 72 hpf, 96 hpf, and 120 hpf. A: anterior, P: posterior. V: ventricle. Scale bar: 10 um. (**D**) Quantification of the fluorescent intensity of the Klf2a (GFP over mCherry) and Notch (GFP over background) reporters in the anterior versus posterior part of the valves at 72 hpf (p=0,001) and p=0,02 respectively), 96 hpf (p=0,005 and p=0,0007 respectively) and 120 hpf (p=0,02 and p=0,01) in wild-type embryos.*

We next investigated the expression of the Hippo effector Yap1 and a reporter of the Hippo pathway *in vivo*. We found that Yap1 is expressed in the heart at 72 hpf, in particular in the OFT smooth muscle cells (Figure 5 A, A'). To better characterize its tissue-specific expression, we used the double transgenic

line *Tg(fli:lifeact-EGFP; kdrl:nls-mCherry)* and could show the smooth muscle cells surrounding the OFT, but also some OFT endothelial cells express Yap1 (asterisks in Figure 5 A'). To assess the activity of the Hippo pathway in the heart at 72 hpf, we made use of the *Tg(4xGTIIC:d2GFP)* and could see that the Yap/Wwtr1-Tead reporter was activated in the OFT endothelial cells as well as the smooth muscle cells surrounding the OFT (Figure 5 B). To assess the implication of Yap1 during OFT valve development, we looked at the valve phenotype in *yap1* mutant embryos (Figure 5 C). When analyzed from 72 hpf until 120 hpf, a significant fraction of *yap1* mutants displayed abnormal valves (17% at 72 hpf, 8% at 96 hpf, 17% at 120 hpf, n=12) and an increasing fraction of *yap1*$^{-/-}$ embryos did not have recognizable OFT valves (58% at 120hpf, n=12). Thus, these results suggest that *yap1* plays an important role during OFT valve morphogenesis (Figure 5 C) and that smooth muscle cell progenitors are likely to play a role in the process.

Together, these results show that Klf2a, Notch signaling, and Hippo pathways are active in the OFT during valve morphogenesis and that Yap1 is essential for OFT valve development.

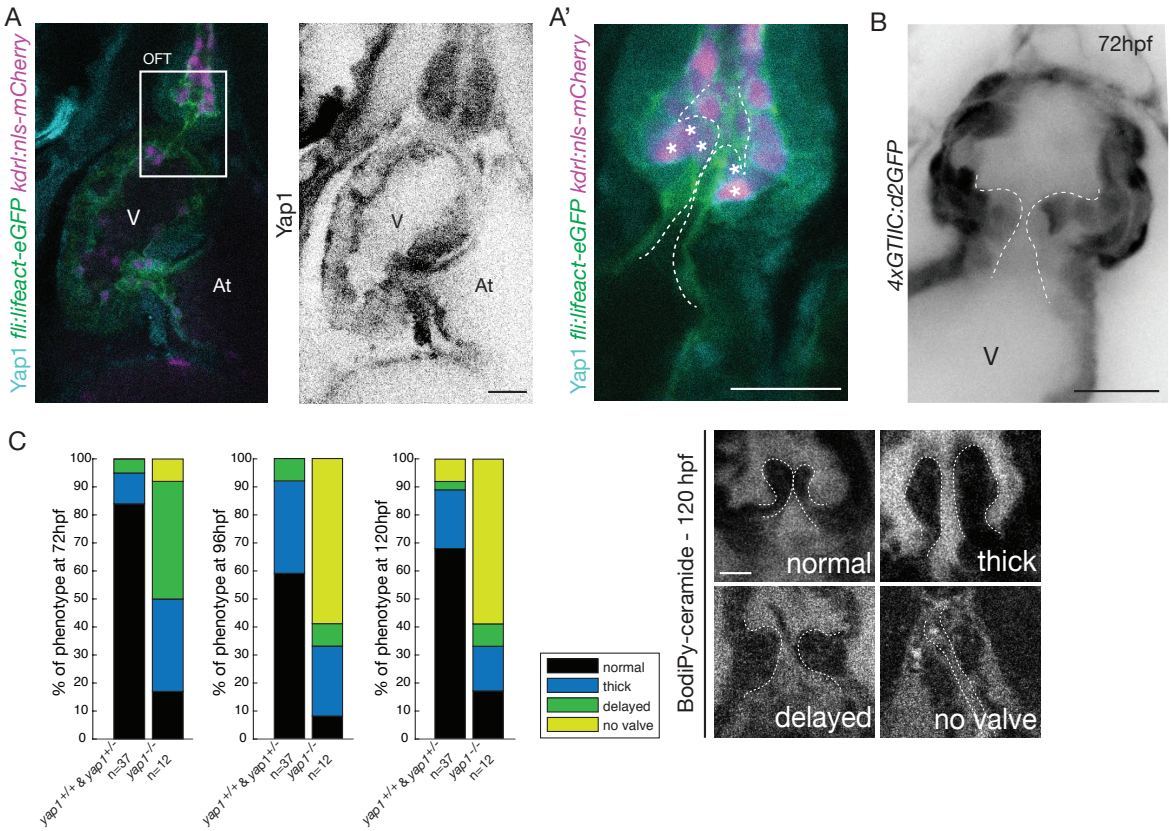


***Figure 5 –Hippo pathway effector Yap1 is active and Yap1 is essential for valve formation in the OFT*** *Yap1 antibody staining on Tg(fli:lifeact-EGFP; kdrl:nls-mCherry) (**A**) and zoom on the OFT (**A'**) at 72 hpf. Asterisks show endothelial cells expressing Yap1. At: atrium, V: ventricle. Scale bar: 20um. (**B**) Confocal z-sections of the TEAD reporter (4xGTIIC:d2GFP) focused on the OFT. V: ventricle. Scale*

*bar: 20 um. (**C**) Example of the valve phenotypes (normal, thick, delayed and no valve) and quantification of the phenotypes in the yap1 controls (yap1$^{+/+}$ and yap1$^{+/-}$) and in yap1$^{-/-}$ mutant embryos. Scale bar: 10 um.*

**Klf2a and Notch reporter activity is flow-dependent in the OFT**

As blood flow is an important regulator of *klf2a* expression and cardiac valve formation, we next wanted to assess whether changes in flow properties impact *klf2a* and the Notch reporter activity in the OFT. We analyzed the reporters activity following injection of a morpholino specific for *troponin T2a* (*tnnt2a*), which is necessary for heart contraction and reliably mimics the *sih* mutants (Sehnert et al., 2002), to determine whether these signaling pathways were impacted when heart contraction is abnormal and/or are activated upon shear stress forces. As the absence of heart contraction can impact heart morphogenesis, we injected highly diluted *tnnt2a* morpholino (hypomorphic condition) into these two reporter lines (Figure 6 A, B). Such treatment allows us to decrease heart function and flow without dramatically altering heart shape (Figure 6 A, B). Depending on the knockdown efficiency in single embryos, this treatment leads to the generation of two groups of embryos: group1 where the heart beats 'normally' (normal heart rate and function) and group2 where the heartbeat is slower. In the group of "beating heart" embryos, we still observe stronger GFP expression in the posterior part of the valve for both reporters at every stage analyzed (Figure 6 A). In the group of embryos where the heart is still beating but at a very slow rate, we observe no difference between the anterior and posterior part of the valve (p=0.99) for the *klf2a* reporter at 72 hpf (Figure 6 B). For the Notch reporter, we observed no difference in fluorescence intensity at 72 hpf (p=0.1) (Figure 6 B). In addition, we analyzed the expression of Fn1, Elnb and Yap1 by immunostaining in both "beating heart" (n=4, n=7 and n=7 respectively) and "slow beating heart" (n=6, n=7 and n=7 respectively) groups and could observe that Fn1, Elnb, and Yap1 are down-regulated in the smooth muscle cells of the "slow beating heart" embryos (Figure 6 C, C'). We next assessed valve morphology in which blood flow is altered due to slow heart contraction and selected the fish with almost no contraction (group2). All the *tnnt2a*MO-injected embryos have no valve (n=9/9) (Figure 6 D). To confirm the role of flow in the process, we analyzed the effect of altered blood viscosity and shear stress by lowering haematocrit content in the *gata1* mutants (*Vlad Tepes*) as previously described (Steed et al., 2016b; Vermot et al., 2009). In *vlad tepes* mutant embryos (n=21), more than 80% of the mutants displayed abnormal OFT valves (Figure 6 D). Together, these results suggest that the expression of both *klf2a* and Notch reporters is flow-dependent and that mechanical forces associated with heart activity are necessary for valve development and smooth muscle cell identity in the OFT.

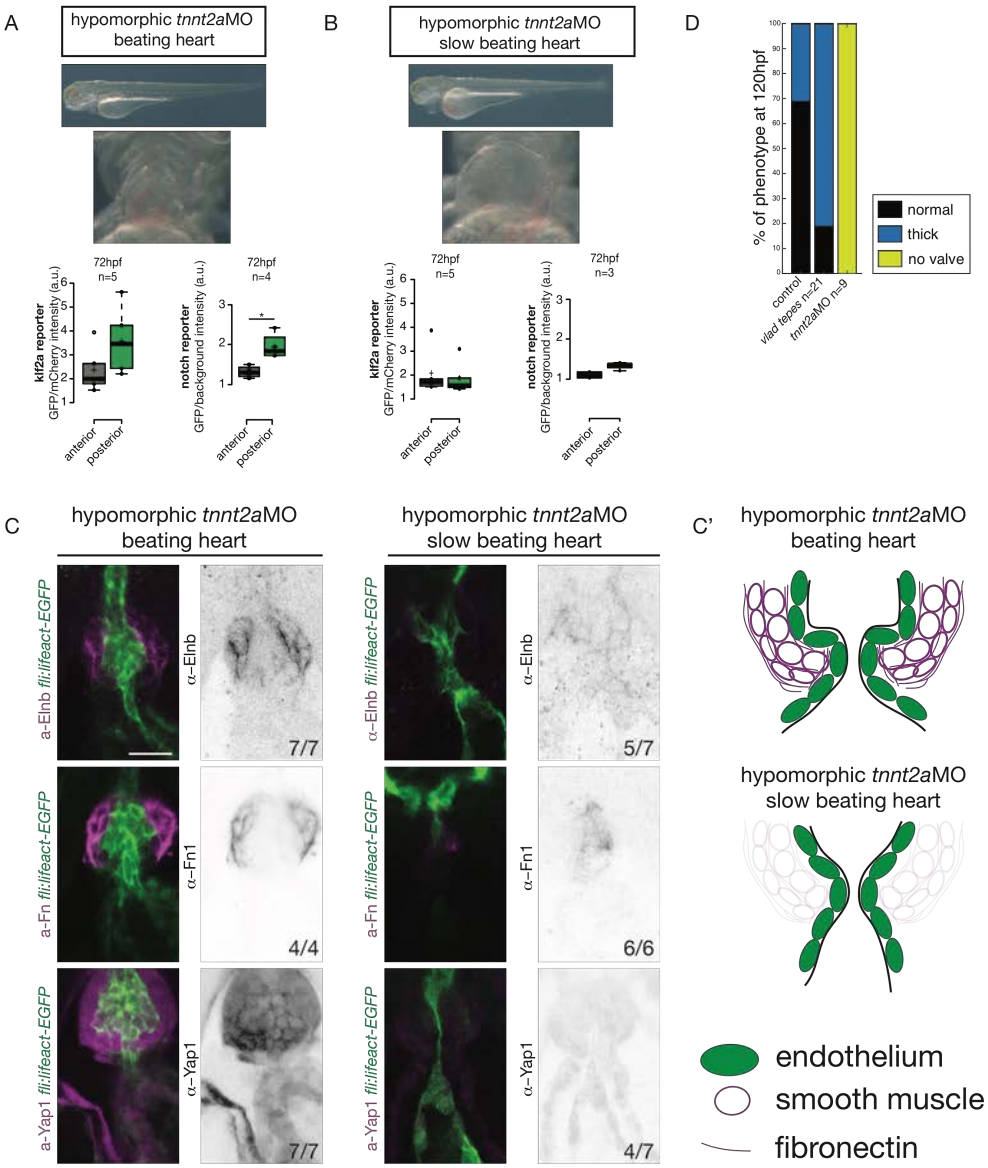


***Figure 6 – Klf2a and notch response, as well as the smooth muscle cell identity, are flow-dependent*** *Quantification of the klf2a and notch reporter expressions in tnnt2a-morpholino injected embryos showing a "beating heart" (p=0,27 and p=0,01 respectively) (**A**) and a "slow beating heart"(p=0,7 and p=0,1 respectively) (**B**) at 72 hpf. (**C**) Z-sections of the Tg(fli:lifeact-eGFP) counterstained with either Fibronectin1 (Fn1), elastin (Elnb) or Yap1 in tnnt2a-morpholino injected embryos (slow beating beating heart). Scale bar: 20 um. (**C'**) Scheme summarizing the down-regulation of the smooth muscle markers in "slow beating heart" embryos compared to "beating heart"embryos. (**D**) Quantification of the phenotypes in the control, vlad tepes mutant (n=21), tnnt2aMO-injected embryos (n=9).*

**Klf2a regulates OFT valve morphogenesis via Notch signaling activation and is necessary for the smooth muscle cells differentiation**

As *notch1b* and *klf2a* are expressed in the OFT endothelium in response to flow forces, we hypothesized that they have a role during OFT valve morphogenesis. Therefore, we imaged the *Tg(fli:gal4/UAS:kaede)* and *Tg(flli:lifeact-EGFP; kdrl:nls-mCherry)* transgenic lines (Figure 7 A, B).

We looked at the phenotype of OFT valve endothelium in the *klf2a*$^{-/-}$ and *notch1b*$^{-/-}$ embryos at 72 hpf, 96 hpf and 120 hpf (Figure 7 A, B). We found that most of the *klf2a*$^{-/-}$ embryos display proper valves at 72 hpf (n=8/11), 96 hpf (n=8/11) and 120 hpf (n=7/11). However, 33% of the *klf2a*$^{-/-}$ embryos have abnormal "delayed phenotype" at 72 hpf (n=4/12), at 96 hpf (n=4/12) and 120 hpf (n=4/12) (Figure 7 A). In this case, the OFT valves are larger, leading to big cushions instead of thin valve leaflets (Figure 7 A). In addition, *notch1b* is also necessary for proper valve formation since 30% (n=6/20) of the *notch1b*$^{-/-}$ embryos have a "delayed phenotype" at 72 hpf, 35% (n=7/10) at 96 hpf and 45% (n=9/20) at 120 hpf (Figure 7 B) while almost all control embryos have proper valves at 72 hpf (n=6/7), 96 hpf (n=7/7) and 120 hpf (n=7/7) (Figure 7 B). Next, we wondered whether a cross-regulation between *notch1b* and *klf2a* exists since they are both necessary for proper valve formation. First, we compared *notch1b* expression between *klf2a*$^{-/-}$ embryos and *klf2a*$^{+/+}$ control embryos (Figure 7 – supplement 1A). In controls, 85% and 91% of the embryos have *notch1b* expression in the OFT at 48 hpf and 72 hpf, respectively (Figure 7 – figure supplement 1 A). However, in *klf2a*$^{-/-}$ embryos, *notch1b* expression is altered with no clear expression defining the OFT region at 48 hpf (64% and 56%) and at 72 hpf (78% and 50%) (Figure 7 – supplement 1 A). However, in the reverse experiment, most of the embryos show proper *klf2a* expression in *notch1b* mutant embryos (61% at 48 hpf and 51% at 72 hpf) (Figure 7 – figure supplement 1B).

In order to assess the regulation of the Notch pathway activity by Klf2a in the endothelium, we analyzed the Notch reporter activity in the posterior and anterior parts of the valve in *klf2a*$^{+/+}$ (n=5) versus *klf2a*$^{-/-}$ (n=4) embryos. As for Notch reporter expression in wild-type (Figure 4 C, D), the Notch reporter is significantly more expressed in the posterior part compared to the anterior part of the valves at 72 hpf (p<10-2), 96 hpf (p<10-2) and 120 hpf (p<10-1) (Figure 7 C, C') in the *klf2a*$^{+/+}$ embryos. Interestingly, the stronger posterior expression is lost in the *klf2a*$^{-/-}$ embryos and the fluorescent intensity in the posterior part of the valve is significantly reduced in the *klf2a*$^{-/-}$ compared to *klf2a*$^{+/+}$ at 72 hpf (p<10-1), 96 hpf (p<$10^{-1}$) and 120 hpf (p<$10^{-1}$) (Figure 7 C, C'). In comparison, the expression in the posterior part of the valve in the *notch1b*$^{-/-}$ embryos compared to the *notch1b*$^{+/+}$ control embryos is not significantly different at any time point analyzed (Figure 7 – figure supplement 1 C). To further assess whether Klf2 has an effect on the OFT formation, we performed Fn1, Elnb and Yap1 stainings on *klf2a*$^{-/-}$ mutants and controls at 72 hpf. We could observe that Fn1, Elnb, and Yap1 are properly expressed in controls (n=13/13, n=7/7 and n=4/4 respectively), *klf2a-/-* (n=5/6, n=3/4, and n=3/3) (Figure 7 – supplement 1 D).

These results suggest that *klf2a* and *notch1b* are necessary for proper valve morphogenesis and that Klf2a regulates *notch* expression in the process. Moreover, *klf2a* does not seem necessary for the smooth muscle cell differentiation surrounding the endothelium.

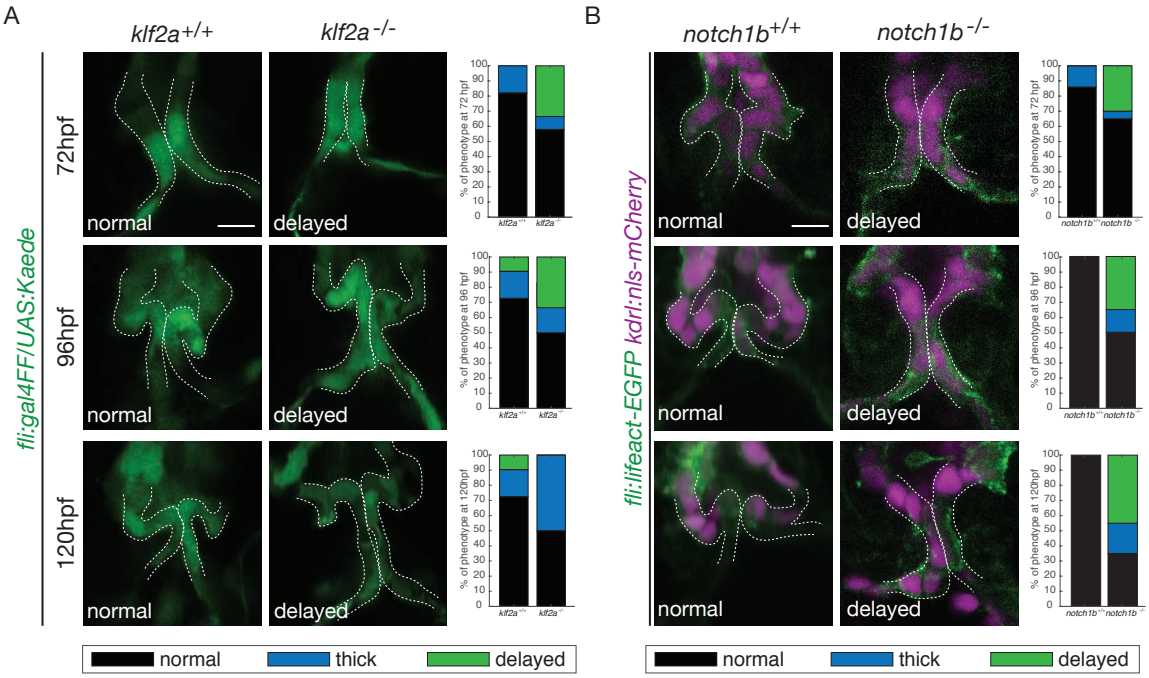


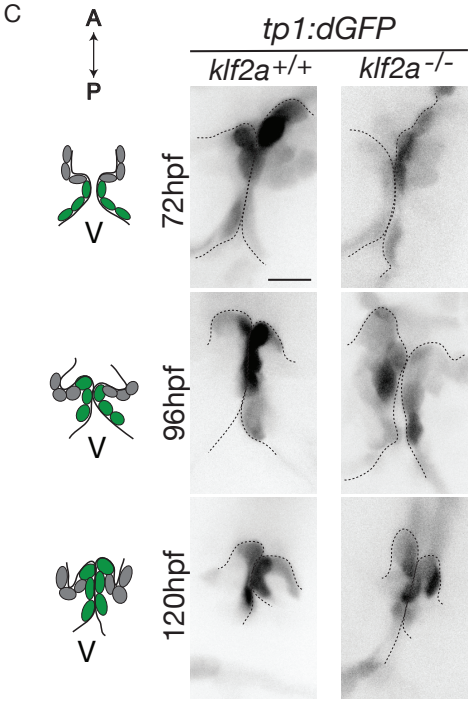


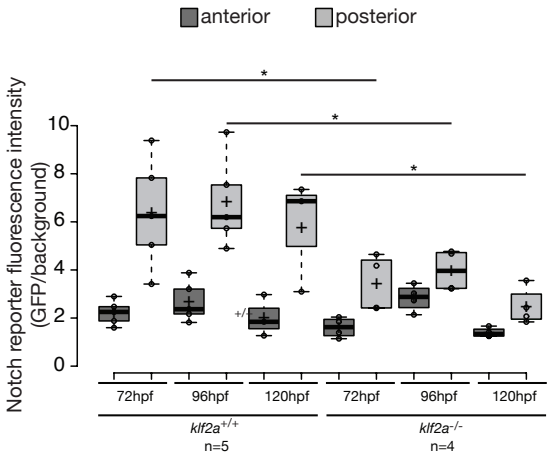

***Figure 7 – Klf2a and notch are necessary for valve formation***

*Quantification of the valve phenotypes at 72 hpf, 96 hpf and 120 hpf (normal, thick, delayed) in klf2a$^{+/+}$(n=11), and klf2a$^{-/-}$ (n=12) using the Tg(fli:gal4FF/UAS:Kaede) (**A**) and notch1b$^{+/+}$ (n=7) and notch1b$^{-/-}$ (n=20) using Tg(fli:lifeact-EGFP; kdrl:nls-mCherry) (**B**) embryos. Scale bar: 10 um. (**C**) Confocal z-sections of the Tg(tp1:dGFP) in klf2a$^{+/+}$ and klf2a$^{-/-}$ embryos at 72 hpf, 96 hpf and 120 hpf. V : ventricle. Scale bar: 10um. (**C'**) Quantification of the fluorescent intensity of the Notch reporter (GFP over background) in the anterior versus posterior parts of the valves in in klf2a$^{+/+}$ (n=5) and klf2a$^{-/-}$ (n=4) embryos. Statistical test were performed to compare the posterior intensities in klf2a$^{+/+}$versus klf2a$^{-/-}$ at 72 hpf (p=0,05), 96 hpf (p=0,03) and 120 hpf (p=0,04).*

**Piezo channels regulate both the endothelial and smooth muscle cell markers expression**

In order to decipher whether flow and mechanosensitive channels could be involved in the regulation the OFT valve formation, we proceeded to analyze the phenotype of different potent mechanosensitive channel mutants. We focused on the non-selective ion channels Trpp2, Trpv4, Piezo1 and Piezo2a (Figure 8 A) that are known for their mechanosensitive properties. First, we evaluated the relative fractional shortening (RFS) in the atrium and in the ventricle of each mutant and their corresponding controls (Figure 8 – figure supplement 1A). We did not observe any significant difference in the RFS between mutants and their respective controls neither in the atrium nor in the ventricle, suggesting that heart function in these mutants is normal. As another readout of flow forces and heart function, we quantified the retrograde flow fraction (RFF) in these mutants and the time windows for forward, reverse or no flow. We found that they are equivalent in all mutants when compared to their respective controls (Figure 8 – figure supplement 1B), confirming that heart function is not different in these mutants. We looked at valve morphology at 120 hpf when leaflets are normally fully formed. In control embryos, the valves are extending into the lumen (Figure 8 A and Figure 8 – figure supplement 1C for individual controls). We found that 33% of the *trpv4* mutant embryos (n=7) have normal valves and mainly display thick valves (67%). In the *trpp2* mutant embryos (n=20), a stronger phenotype is observed with only 10% of normal valves. We observe that some embryos are delayed with respect to valve phenotype, meaning that the valve forming area still displays cushions at 120 hpf instead of having leaflets (35%). The *trpv4$^{-/-}$; trpp2$^{+/-}$* (n=8) has an intermediate phenotype with 25% of the embryos having normal valves. Finally, the *trpp2$^{-/-}$; trpv4$^{-/-}$* embryos (n=11) have a stronger phenotype, with none of the embryos showing proper OFT valve development and displaying mainly a delayed valve phenotype (45%). Interestingly, the *piezo1* mutant embryos (n=14) show mainly a delayed valve formation (50%), similarly to the *trpv4$^{-/-}$; trpp2$^{-/-}$* embryos. The *piezo2a$^{-/-}$* (n=9) has a less stringent phenotype with mainly normal valves (44%) but nevertheless 11% of *piezo2a$^{-/-}$* fish do not have valves at all. This phenotype is even more prevalent in *piezo1$^{-/-}$; piezo2a$^{-/-}$* embryos (n=11), where none of the fish display proper valve development and most of them do not form any valves (36%).

To better characterize the valve phenotype in *trpp2$^{-/-}$* and *piezo1$^{-/-}$* embryos, we made use of the *Tg(fli:lifeact-EGFP; kdrl:nls-mCherry)* transgenic line and assessed the shape of the endothelium at 72 hpf (Figure 8 B and Figure 8 – supplement 2, 3), 96 hpf (Figure 8 C and Figure 8 – supplement 2, 3)

and 120 hpf (Figure 8 D and Figure 8 – supplement 2, 3). *Trpp2*$^{-/-}$ embryos display mainly thick valves at all timepoints (n=4/8 at 72 hpf, n=8/13 at 96 hpf and n=5/11 at 120 hpf) (Figure 8 B-D and Figure 8 – supplement 2). Indeed, the endothelial layer is not a single cell layer anymore (Figure 8 C) which leads to a thicker leaflet at 120 hpf (Figure 8 D). Although *piezo1*$^{-/-}$ embryos have mainly normal valves at 72 hpf (Figure 8 B and Figure 8 – supplement 3) (n=7/10), they display a delayed phenotype (still cushions) at 96 hpf (Figure 8 C and Figure 8 – supplement 3) (n=4/10 and thick or delayed phenotype at 120 hpf (Figure 8 D and Figure 8 – supplement 3) (n=3/10 and n=3/10 respectively) (Figure 8 B). These results suggest that Trp and Piezo channels are necessary for the proper folding of the endothelium from 72 hpf to 120 hpf.

To better characterize the cell layer affected by piezo loss of function, we performed immunohistochemistry against Yap1 and two smooth muscle identity markers (Fn1 and Elnb) in *piezo1*$^{+/+}$ controls and *piezo1*$^{-/-}$ mutants at 72 hpf (Figure 8 E). A large fraction of *piezo1*$^{-/-}$ embryos (n=7/10) display reduced Yap1 expression as well as a down-regulation of Elnb (n=9/12) and Fn1 (n=3/4) (figure 8 E). These results suggest an important role of *piezo1* in the regulation of the smooth muscle cell identity and proper gene expression in the OFT. We next assessed Klf2a reporter expression in *piezo1*$^{-/-}$ and *trpp2*$^{-/-}$. We found that klf2a expression was misregulated in *piezo1*$^{-/-}$ mutant embryos with stronger Klf2a reporter activation in the anterior and posterior part of the valve endothelium when compared to controls ($p<10^{-3}$ for the anterior part and $p<10^{-2}$ for the posterior part of the valves) (Figure 8 F, F'). By contrast, we found that the posterior part of the valve has a decreased expression of GFP ($p<10^{-2}$), highlighting a down-regulation of *klf2a* in the *trpp2*$^{-/-}$ embryos (Figure 8 G, G'). These results suggest that Piezo1 inhibits *klf2a* overall the valve endothelium (Figure 8 F, F') while Trpp2 is required for *klf2a* activation in the posterior part of the OFT valve endothelium (Figure G, G'). We conclude that Piezo1 plays a dual role in the OFT: it modulates *klf2a* expression in the endothelium and it is necessary for proper smooth muscle cell identity around the OFT endothelium.

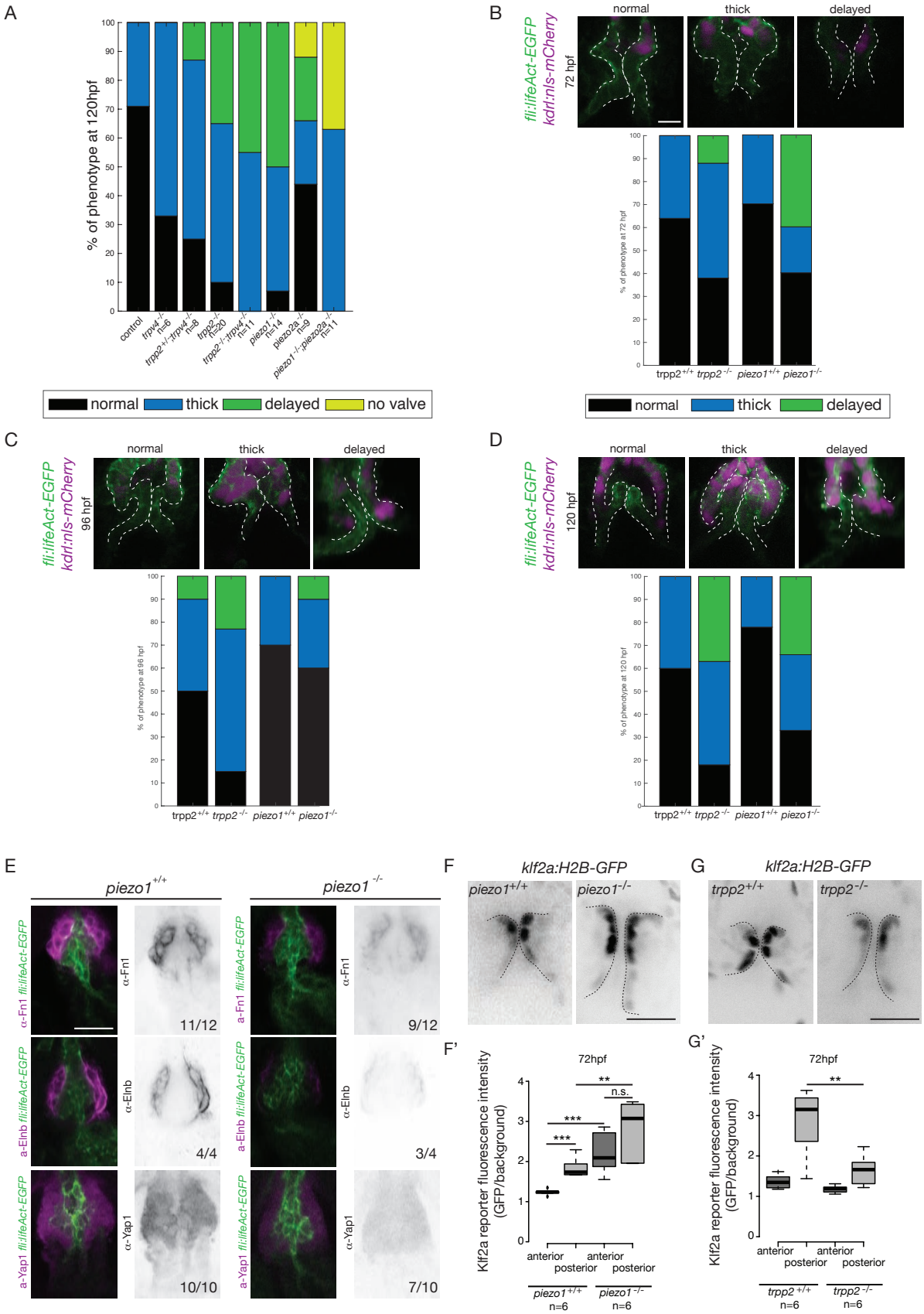


***Figure 8 – Flow and mechanosensitive channels are necessary for proper OFT valve formation***

*(A) Quantification of the valve phenotypes at 120 hpf (normal, thick, delayed and no valve) in control, trpv4$^{-/-}$ (n=6), trpp2$^{+/-}$; trpv4$^{-/-}$ (n=8), trpp2$^{-/-}$ (n=20), trpp2$^{-/-}$; trpv4$^{-/-}$ (n=11), piezo1$^{-/-}$ (n=14), piezo2a$^{-}$*

*$^{-/-}$ (n=9), piezo1$^{-/-}$; piezo2a$^{-/-}$ (n=11). Z-sections and quantifications of the valves phenotypes (normal, thick, delayed) of the Tg(fli:lifeaAct-EGFP; kdrl:nls-mCherry) at 72 hpf (**B**), 96 hpf (**C**) and 120 hpf (**D**) in trpp2$^{+/+}$(n=11, n=10, n=10), trpp2$^{-/-}$ (n=8, n=13, n=13), piezo1$^{+/+}$ (n=10, n=10, n=9) and piezo1$^{-/-}$ (n=10, n=10, n=9 respectively). Scale bar: 10 um. (**E**) Fibronectin1 (Fn1), elastin (Elnb) and Yap1 staining on Tg(fli:lifeact-eGFP) in piezo1$^{+/+}$ (n=12, n=4 and n=10 respectively) and piezo1$^{-/-}$ (n=12, n=4 and n=10 respectively). Scale bar: 20 um. Z-sections (**F**) and quantification (**F'**) of the klf2a reporter (GFP over background) in the anterior and posterior parts of the valves in piezo1$^{+/+}$ (n=6) and piezo1$^{-/-}$ (n=6). Scale bar: 20 um. Z-sections (**G**) and quantification (**G'**) of the klf2a reporter (GFP over background) in the anterior and posterior parts of the valves in trpp2$^{+/+}$ (n=6) and trpp2$^{-/-}$ (n=6). Scale bar: 20 um.*

## Discussion

Using cardiac live imaging and functional studies combined with *in vivo* reporter analysis, we uncover key mechanosensitive signaling pathways involved in OFT valve morphogenesis (Figure 9). We identify two tissue layers sensitive to mechanical forces in the OFT: (1) The endothelial cells where *klf2a* expression is modulated both by Piezo and Trp channels (2) The smooth muscles surrounding the endothelium, where Piezo channels regulate Yap1 expression and smooth muscle cell identity (Figure 9). These observations enable us to confirm the universal role of mechanical forces in cardiac valve morphogenesis and suggest a unique mechanism for OFT valve morphogenesis in which the origins of the valve progenitors, the implication of particular groups of cells, the mechanosensors involved and the impact of the mechanotransduction cascade are identified.

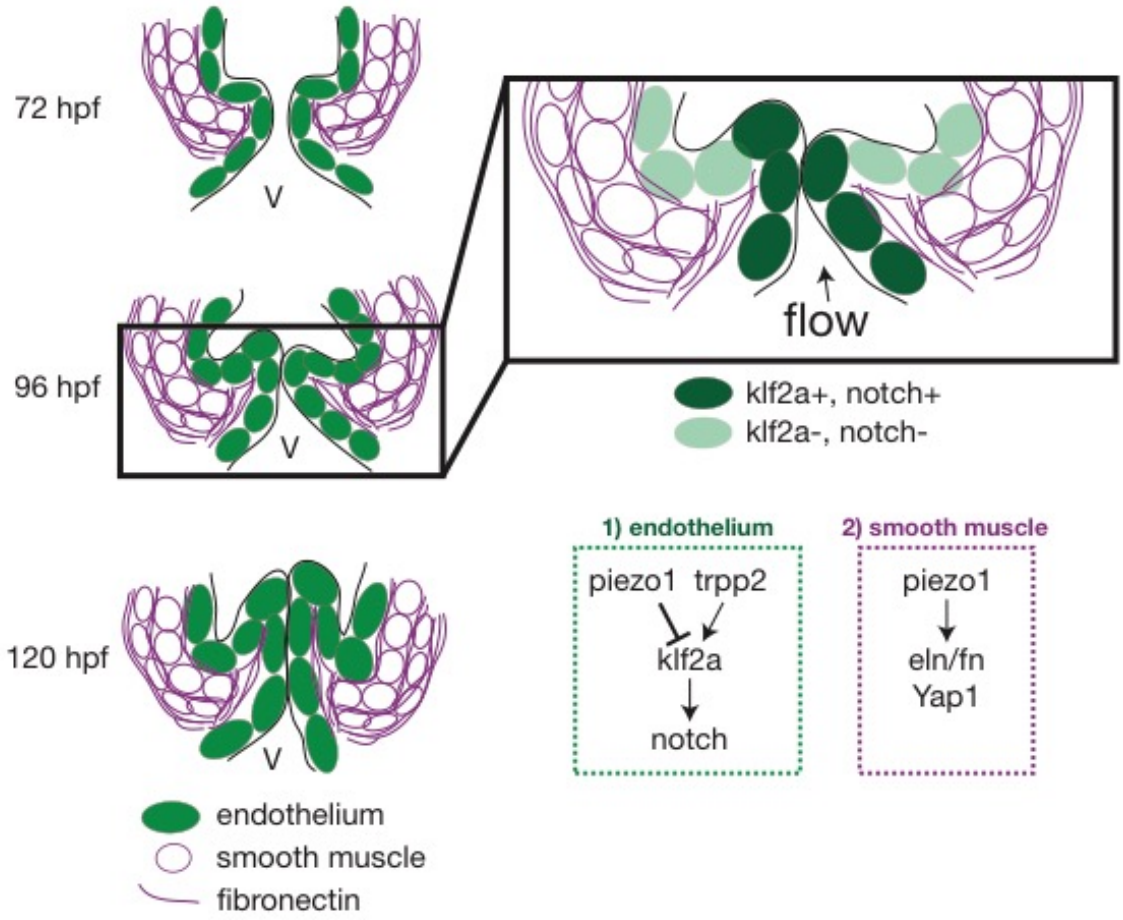


**Figure *9 – Mechanosensitive signaling pathways during OFT valve morphogenesis***

*Two cell layers forming the OFT valves respond to piezo1 activity: the endothelium (green) and smooth muscle cells (magenta). In the endothelium, Klf2a modulates Notch signaling and Piezo1 represses Klf2a while Trpp2 activates it. In the smooth muscle cells, Piezo1 regulates the expression of elastin (eln), fibronectin (fn) and Yap1.*

**Klf2a modulates Notch signaling specifically in the OFT endothelium**

Valve morphogenesis occurs in complex mechanical environments. In the AVC, endocardial cells experience both shearing forces and mechanical deformation due to the contraction of the heart and its associated blood flow. The situation is slightly different in the OFT because endothelial valvular progenitors are not surrounded by contractile cardiomyocytes but passive smooth muscle cells. Here, we show that the main mechanosensitive pathways involved in AVC valve development are required for OFT valve development, even though the mechanical stimuli vary greatly between these two sets of valves. Previous studies have proposed that *klf2a* and *notch1b* are important during the formation of functional cardiac valve leaflets in zebrafish. Both are specifically expressed in the AVC (Beis et al., 2005; Pestel et al., 2016; Steed et al., 2016b; Vermot et al., 2009) and are transcriptionally misregulated in models of Cerebral cavernous malformation (CCM) where cardiac valve development is altered

(Donat et al., 2018). Here, we show that both Notch signaling and *klf2a* are active in the endothelial cells of the OFT between 48 hpf and 120 hpf. During the process in which zebrafish cardiac AVC cushion remodel into valve leaflets, endocardial *klf2a* expression and Notch activity are high on the luminal side of the developing valve leaflet, which is exposed to blood-flow, whereas their expression is lower on the abluminal side of the leaflet (Pestel et al., 2016; Steed et al., 2016b). In the OFT, *klf2a* expression and Notch activation follow a different pattern because we could not clearly identify abluminal cells in the OFT. This might reflect a complete lack of endothelial to mesenchymal transition in the OFT by comparison to the AVC. Nevertheless, the impact of both pathways on valve morphogenesis remains the same as we found that *klf2a*$^{-/-}$ and *notch1b*$^{-/-}$ embryos show similar valve phenotypes and Notch signaling pathway is significantly decreased in *klf2a*$^{-/-}$ mutants. Even though the downstream players of the notch pathway remain to be established in the OFT, these results validate previous observations, suggesting that *klf2a* acts upstream of *Notch* signaling in the endocardium (Donat et al., 2018; Samsa et al., 2015; Vermot et al., 2009). Considering that Notch has been proposed to be mechanosensitive in blood vessels (Mack et al., 2017), an attractive hypothesis is that the Klf2-Notch axis could be a general mechanosensitive cascade in endothelial cells. In that case, it would be interesting to address *notch* activity in a flow related context, similarly to what is currently being done with Nf-kb, Klf2a, and other flow responsive pathways (Feaver et al., 2013). This assumption is particularly interesting in the context of sprouting angiogenesis and other aspects of angiogenesis where Notch is broadly required (Choi et al., 2017; Hasan et al., 2017; Pitulescu et al., 2017; Tammela et al., 2011). We further show that the expression of Fibronectin1 and Elastinb in the smooth muscle cells surrounding the OFT is not altered in the *klf2a*$^{-/-}$mutants. Considering that Piezo is emerging as an important contributor to human diseases related to blood cells (Ma et al., 2018; Zarychanski et al., 2012) and lymphatic diseases in humans (Lukacs et al., 2015), our work should motivate the search of potential involvement of Piezo in cardiac pathologies such as valvulopathies.

**Piezo is necessary for OFT smooth muscle cell identity and endothelial *klf2a* expression in the OFT**

Cardiac valve development is highly dependent on endothelial/endocardial cell mechanosentivity. Previous work identified the membrane-bound mechanosensitive channels (Trpp2 and Trpv4) and a calcium-activated intracellular signaling cascade leading to *klf2a* expression and valve morphogenesis as key elements of the endocardial mechanodetection-signaling pathway. Consistently, we found that these TRP channels are also required for endothelial *klf2a* expression and OFT valve formation. In addition, we identify another type of mechanosensitive channel belonging to the Piezo family. Piezo channel mutants show a dramatic valve phenotype, suggesting a crucial role during OFT valve morphogenesis. Interestingly, Piezo channels are important both for modulating *klf2a* expression in the endothelium and for smooth muscle cell-specific expression of Elnb and Fn1. Piezo function in these two cell layers is consistent with the fact that Piezo1 is expressed in smooth muscle cells and is important

for tissue remodeling in mouse arteries (Retailleau et al., 2015) as well as in endothelial cells in mouse vasculature (Li et al., 2014; Ranade et al., 2014) and lymphatic valves (Nonomura et al., 2018). These studies along with our results suggest that Piezo1 might be necessary for both layers to regulate distinguishable functions: activation of signaling cascade upon shear stress in the OFT endothelium and proper cell identity acquisition in smooth muscles. Both tissue layers might be sensing different stimuli: shear plus strain for the endothelial cells and strain for the smooth muscle cells. This hypothesis is consistent with the fact that Piezo is sensitive to stretch (Ranade et al., 2015), compression (Lee et al., 2014; Qi et al., 2015), and rhythmic mechanical stimuli (Lewis et al., 2017). Importantly, Piezo-dependent can transduce forces at the cell-cell or cell-matrix interface (Eisenhoffer et al., 2012; Poole et al., 2014). Thus, Piezo can have different mechanosensitive roles both in smooth muscle cells and endothelium to coordinate the expression of klf2 and ECM proteins.

**Yap1 and Hippo pathways are regulators of the OFT valve formation in the endothelium and smooth muscles**

Our work shows that Yap1 is specifically expressed in the OFT in both endothelial cells and smooth muscle cells and is required for valvulogenesis. Accordingly, the Hippo pathway is active in smooth muscles and in the endothelium. Our work suggests that Piezo constitutes a plausible regulator of Yap1 expression as Piezo1 seems important for both endothelium and smooth muscle identity. Interestingly, Yap1 has been shown to translocate less in the nucleus in Piezo1 mutant mice neural stem cells (Pathak et al., 2014) and to induce proliferation in smooth muscles during cardiovascular development in mouse (Wang et al., 2014). Even though we were not able to assess Yap1 subcellular localization *in vivo*, the regulation of YAP1 activity and ECM assembly might be a general feature of Piezo function. The connection between Piezo and Yap1 is particularly interesting in the context of OFT development and function. In teleost, the OFT has an important biomechanical role for the control of flow propagation within the vascular networks by contributing to the dampening of the pressure wave down the arterial tree (Braun et al., 2003b). In zebrafish, Yap1 is involved in the determination of cardiac precursor cells into smooth muscle cell fate via a process that involves the regulation of Elastinb expression (Moriyama et al., 2016). Besides the control of cell identity, ECM contributes to biomechanical properties of tissues (Dzamba and DeSimone, 2018). It is thus possible that piezo is a major regulator of tissue mechanical properties by regulating Yap1 expression. In the vascular system, Yap1 is necessary for vessel stability in response to flow (Nakajima et al., 2017) and is required for maintaining junctional integrity and endothelial cell rearrangements in angiogenic vessels in response to stretch (Neto et al., 2018). It will be interesting to see if these functions also rely on the modulation of the expression of ECM proteins by the Piezo-Yap1 axis in angiogenic contexts. Similarly, the downstream targets of piezo are not identified in the lymphatic valves and a number of flow responsive transcription factors such as foxc2 and Nfat1 (Sabine et al., 2012; Sabine et al., 2015; Sweet et al., 2015) are normally expressed of piezo mutants (Nonomura et al., 2018).

## Material and methods

### Zebrafish strains, husbandry, embryo treatments, and morpholinos

Animal experiments were approved by the Animal Experimentation Committee of the Institutional Review Board of the IGBMC. Zebrafish lines used in this study were *Tg(fli1a:lifeact-EGFP)* (Phng et al., 2013), *Tg(kdrl:nls-mCherry)* (Nicenboim et al., 2015), *Tg(kdrl:EGFP)* (Jin et al., 2005), *Tg(fli1a:nls-mCherry)* (Heckel et al., 2015), *Tg(myl7:egfp)* (Huang et al., 2003), Tg(*−26.5Hsa.WT1-gata2:eGFP)*$^{cn12}$ (Sanchez-Iranzo et al., 2018), *Tg(klf2a(6kb):H2B-eGFP)* (Heckel et al., 2015), *Tg(tp1:dGFP)* (Ninov et al., 2012), *Tg(4xGTIIC:d2GFP*) (Miesfeld and Link, 2014), *vlad tepes*$^{m651}$ (Lyons et al., 2002), *cup*$^{tc321}$ (Schottenfeld et al., 2007), *piezo1*$^{sa12608}$ (EZRC), *piezo2a*$^{sa12414}$ (ZIRC), *trpv4*$^{sa1671}$ (ZIRC), *notch1b*$^{sa11236}$ (ZIRC), *klf2a*$^{ig4}$ (Steed et al., 2016b), *yap1*$^{fu48}$ (Agarwala et al., 2015) and wild-type AB. Cup mutant embryos were phenotyped based on the curled tail phenotype. All animals were incubated at 28.5 °C for 5 h before treatment with 1-phenyl- 2-thiourea (PTU) (Sigma Aldrich) to prevent pigment formation. Morpholino specific for *tnnt2a* (Sehnert et al, 2002) (5'-CATGTTTGCTCTGATCTGACACGCA-3') were obtained from GeneTools. It was injected into the yolk at the one-cell stage at a concentration of 5,8ng to stop the heart. It was diluted 40 times in order to get fish with either a decreased heartbeat ("slow beating heart" group in this study) or close to the non-injected fish heartbeat ("beating heart" group in this study).

### Immunofluorescence

Embryos were fixed at the desired stage in 4% paraformaldehyde overnight at 4 °C. After washing in 1X PBST (PBS-0.1% Tween-20), embryos were permeabilized in 1X PBST containing 1% Triton-X 100 for 30 min at room temperature or overnight at 4 °C. For Fibronectin1 staining, the pericardial cavity was then carefully pierced with the tip of a needle to facilitate antibody penetration before blocking in permeabilization buffer supplemented with 5% BSA. Embryos were incubated in blocking solution containing 5% BSA and 15% NGS (anti-Fn1), 1% BSA, 2% NGS (anti-Elnb) and 2% BSA, 2% MgCl2 (1M), 5% NGS supplemented by 1,5% Tween-20 (anti-Yap1) for 2 h at room temperature or overnight at 4 °C. Primary antibodies were added to the relevant blocking solution and incubated 2 overnights at 4 °C. Secondary antibodies were added in blocking solution after thorough washing in PBST and incubated for 2 days at 4 °C. Embryos were thoroughly washed in PBST and mounted for imaging on a Leica SP8 confocal. Antibodies were used as follows: rabbit anti-Fn1 (F3648, Sigma) 1:100, rabbit anti-Elnb (Miao et al., 2007, kind gift from Burns lab, Paffett-Lugassy, N., et al. (2017)) 1:1000, rabbit anti-Yap1 (generated by the Lecaudey lab) 1:300 and Alexa Fluor™ 647 goat anti-rabbit IgG secondary antibody (A21245, Life Technologies) were used at 1:500.

### In situ hybridization

*In situ* hybridization was performed as in Thisse &Thisse, 2008. Anti-sense probes for *notch1b* and *klf2a* were generated from a plasmid containing the cDNA of zebrafish *notch1b* in pCR-script SK+ (provided by the Bakkers lab, The Netherlands) and zebrafish *klf2a* in IRBOp991B0734D (provided by RPDZ, Berlin) and subsequently transcribed using the T3 polymerase and T7 polymerase, respectively. After ISH, embryos were incubated subsequently in 45% and 90% D-fructose (Sigma F0127) containing 0,5% of 1-Thioglycerol (Sigma M6145) for 20 minutes. Imaging of ISH was done using a Leica M165 macroscope with a TrueChrome Metrics (Tucsen) with a Leica 1.0X objective (10450028).

**Confocal imaging**

For live imaging, zebrafish embryos were staged, anaesthetized with 0.02% tricaine solution or 50 mM BDM, to stop the heart when necessary, and mounted in 0.7% low melting-point agarose (Sigma Aldrich). Confocal imaging was performed either on a Leica SP8 confocal microscope (experiments with BODIPY-ceramide or fixed samples) or a Leica spinning disk (valve structure, flow profile, reporter experiments). Fast confocal imaging to image valve leaflets from 72 hpf to 120 hpf stained with BODIPY-ceramide was performed using the resonant scanner mode of the Sp8 microscope. Images were acquired with a low-magnification water immersion objective (Leica HCX IRAPO L, 25X, N.A. 0.95). The optical plane was moved 2 um between the z-sections until the whole OFT was acquired. 2-colored fast confocal imaging was used to image valve structure, red blood cells, and reporter activities from 56 hpf to 144 hpf was performed using a Leica DMi8 combined with a CSU-X1 (Yokogawa) spinning at 10 000 rpm, 2 simultaneous cameras (TuCam Flash4.0, Hamamatsu) and a water immersion objective (Leica 20X, N.A. 0.75 or Leica 40X, N.A. 1.1). 1ms exposure was used for red blood cells imaging and 20ms exposure for valve structure and reporter activity experiments. 50 % of 488 laser power and 40 % of 561 laser power were used for reporter activity experiments.

**BODIPY-ceramide imaging**

Embryos were incubated with 4 mM BODIPY-ceramide (Molecular Probes) overnight and then processed as in Heckel et al., 2015 and Vermot et al. 2009 to visualize the valve shape.

**Photoconversion**

Photoconversion was performed using the FRAP module on a SP8 confocal microscope and a Leica HCX IRAPO L, 25X, NA0.95 water immersion objective. *Tg(fli1a:Gal4FF; UAS:Kaede)* embryos were mounted in 0.7% low melting-point agarose supplemented with 50 mM BDM to inhibit heart contraction for the duration of the procedure. A region of interest corresponding to the anterior, middle or posterior part of the valve was selected and exposed to 405 nm light (25% laser power). One pre-bleach frame was acquired, followed by 3–6 bleach pulses (3–5 ms each) without acquisition to achieve conversion of the kaede protein to its red form. A z-stack of the photoconverted heart was then acquired in the standard confocal mode to record the starting point of each experiment. Embryos were then carefully

dissected from the agarose, placed in fish water for 5–10 min until heart contraction resumed and then put at 28.5 °C to develop individually under standard conditions until the next time point of interest.

**Fractional shortening**

Imaging was performed on a Leica DMIRBE inverted microscope using a Photron SA3 high-speed CMOS camera (Photron, San Diego, CA) and water immersion objective (Leica 20X, NA 0.7). Image sequences were acquired at a frame rate of 1000 frames per second. FS% = (Dm diastole- Dm systole)/ (Dm diastole) and where Dm is the diameter of the chamber of interest (atrium or ventricle).

**Flow analysis**

Red blood cells were manually tracked through the OFT and their velocity calculated from image sequences of the *Tg(gata1:ds-red; kdrl:eGFP)* beating heart, acquired at 1000 frames per second as described previously. Red blood cells transiting through the OFT were tracked manually on Imaris and their velocity calculated. The tracks of multiple cells in at least 4 embryos per stage were assembled to obtain an estimate of the flow velocity over multiple cardiac cycles (typically 3). Velocities estimated at the same time point by tracking different cells were averaged.

**Image analysis**

For fluorescence intensity analysis of the Klf2a reporter, the *Tg(klf2a:H2B-eGFP)* reporter line was crossed with the *Tg(fli1a:nls-mCherry)* line and the mCherry signal was used for normalization. The maximum intensity of each channel was quantified and the GFP over mCherry ratio generated. For fluorescence intensity analysis of the Notch reporter, the ratio of the maximum intensity of the GFP signal from the *Tg(tp1:dGFP)* reporter line over the maximum intensity of the background was generated.

These ratios were then averaged for three cells in the anterior part and three cells in the posterior part of both valves in the OFT of individual embryos. Finally, the averages of the anterior and posterior parts were compared.

**Statistical analyses**

We did not compute or predict the number of samples necessary for statistical differences because the standard deviation of our study's population was not known before starting our analysis. Biological replicate corresponds to the analysis of different embryos of the same stage. Technical replicate corresponds to the analysis of the same embryo imaged the same way. The sample size (biological replicate and number) to use was as defined by our ability to generate our datasets. For analyses between two groups of embryos, differences were considered statistically significant when the p-value<0.05, as determined using a two-tailed and paired Student's t-test. For boxplots, center lines show the medians, crosses show the means, box limits indicate the 25th and 75th percentiles as determined by R software;

whiskers extend 1.5 times the interquartile range from the 25th and 75th percentiles, data points are represented as circles.

## Supplementary figures

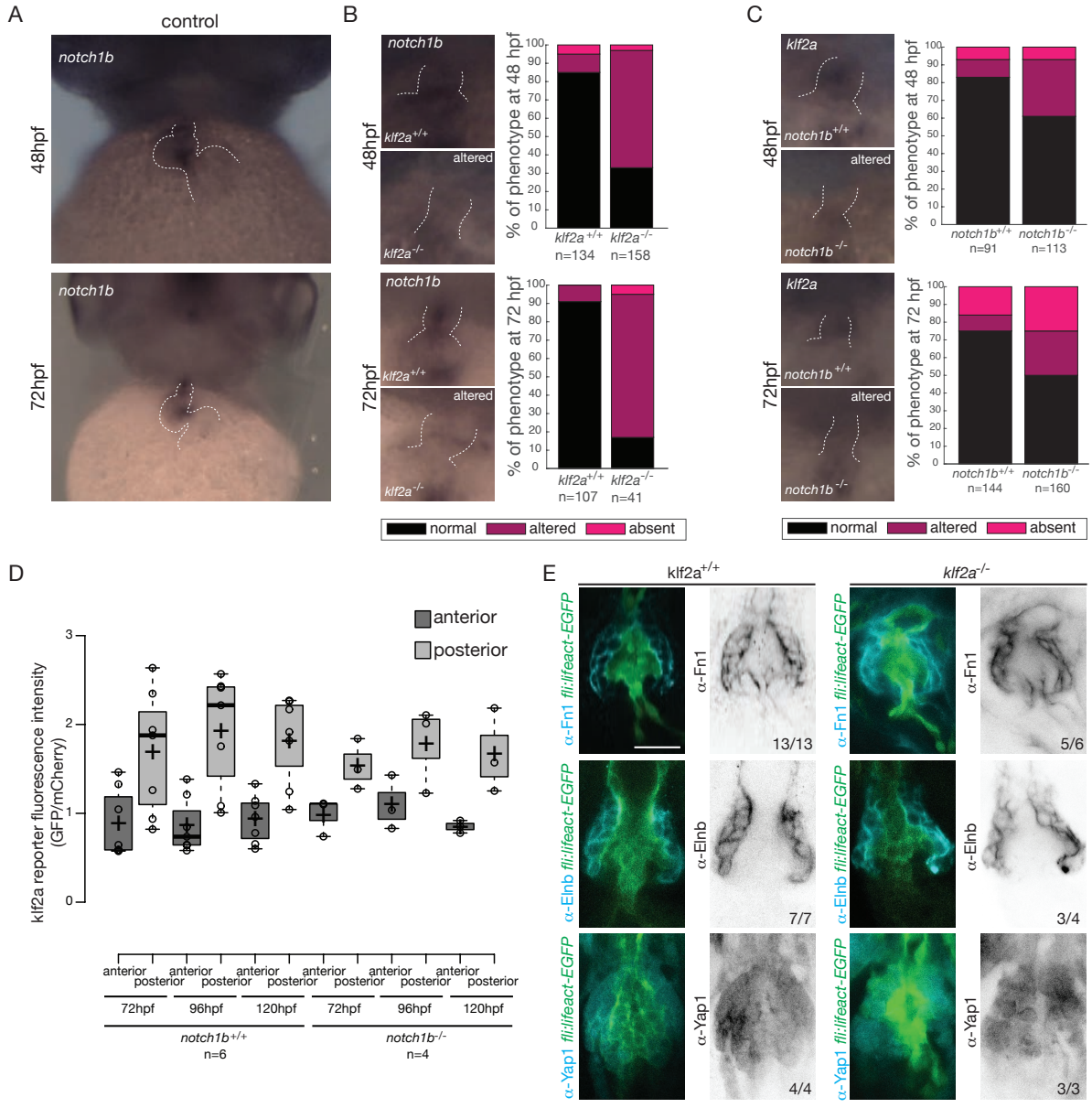


**Figure 7 – figure supplement 1 – Klf2a regulates notch1b expression but Notch1b does not regulate klf2a expression**

*In situ hybridization* of *notch1b* in *klf2a*$^{+/+}$ (n=134 and n=107 at 48 hpf and 72 hpf respectively) *and klf2a*$^{-/-}$ (n=158 and n=41 at 48 hpf and 72 hpf respectively) *embryos (**A**) and of klf2a* in *notch1b*$^{+/+}$ (n=91 and n=144 at 48 hpf and 72 hpf respectively) and *notch1b*$^{-/-}$ (n=113 and n=160 at 48 hpf and 72 hpf respectively) embryos (**B**) and quantification of their expression pattern in the OFT at 48 hpf. (**C**) Quantification of the fluorescent intensity of the Klf2a reporter (GFP over mCherry) in the anterior versus posterior part of the valves at 72 hpf, 96 hpf and 120 hpf in *notch1b*$^{+/+}$ (n=6) and *notch1b*$^{-/-}$ (n=4)

embryos using the *Tg(klf2a:H2B-GFP; fli:nls-mCherry)* transgenic line. ***(D)*** *Fibronectin1 (Fn1), elastin (Elnb) and Yap1 immunostaining on Tg(fli:lifeact-eGFP) in control (n=13, n=7, n=4 respectively), klf2a*$^{-/-}$ *(n=6, n=4, n=3 respectively). Scale bar : 20 um.*

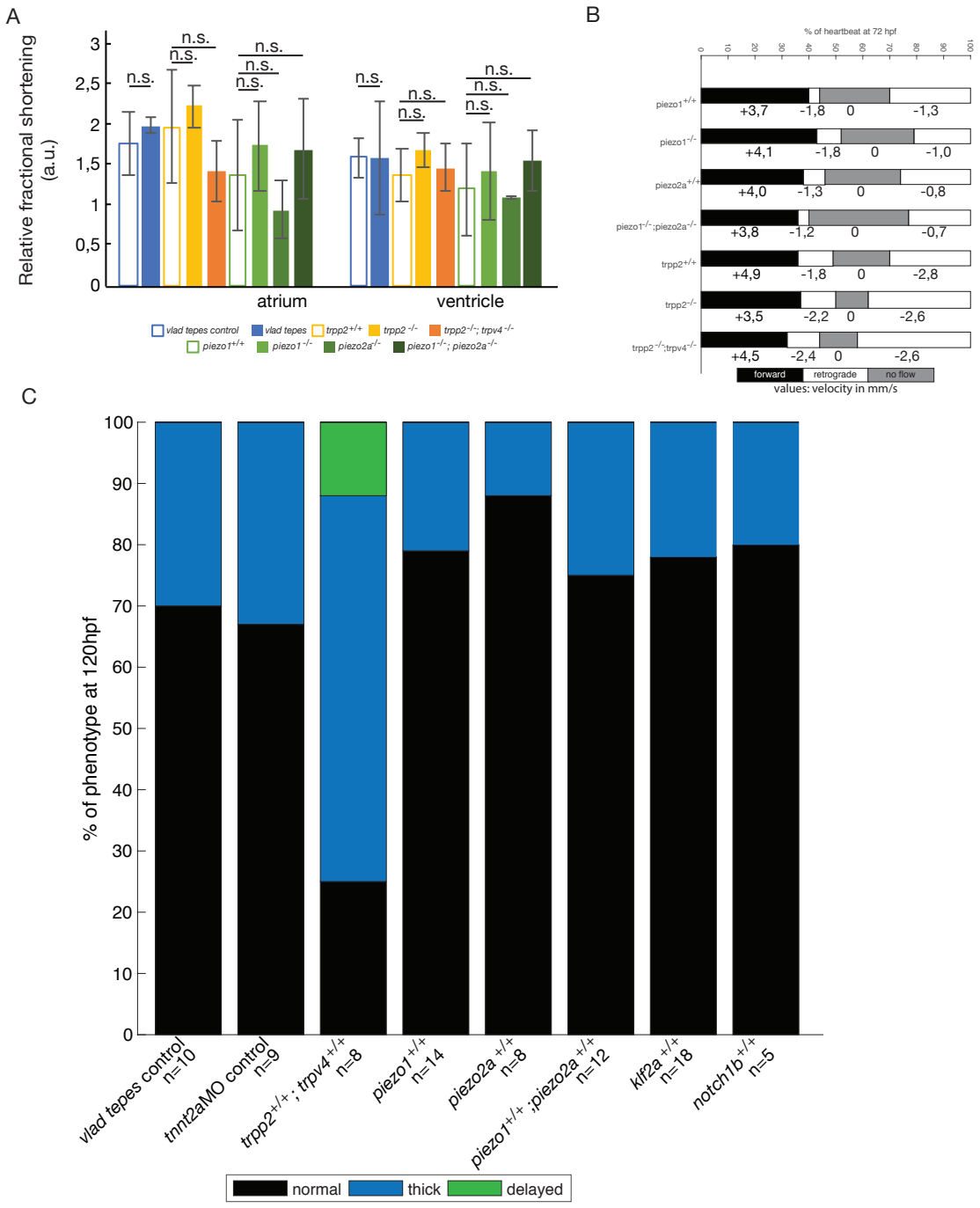


***Figure 8 – figure supplement 1 – Valve phenotypes in controls***

*(**A**) Relative fractional shortening in the atrium and ventricle in control, vlad tepes mutant, trpp2-/-, trpp2-/-; trpv4-/-, piezo1-/-, piezo1-/-; piezo2a-/-. (**B**) Flow profile in the OFT at 72 hpf in the same*

*mutants showing the forward flow (green), retrograde flow (magenta) and no flow (grey) fractions. (**C**) Quantification of the phenotypes in the respective mutant controls from Figure 7 at 120 hpf.*

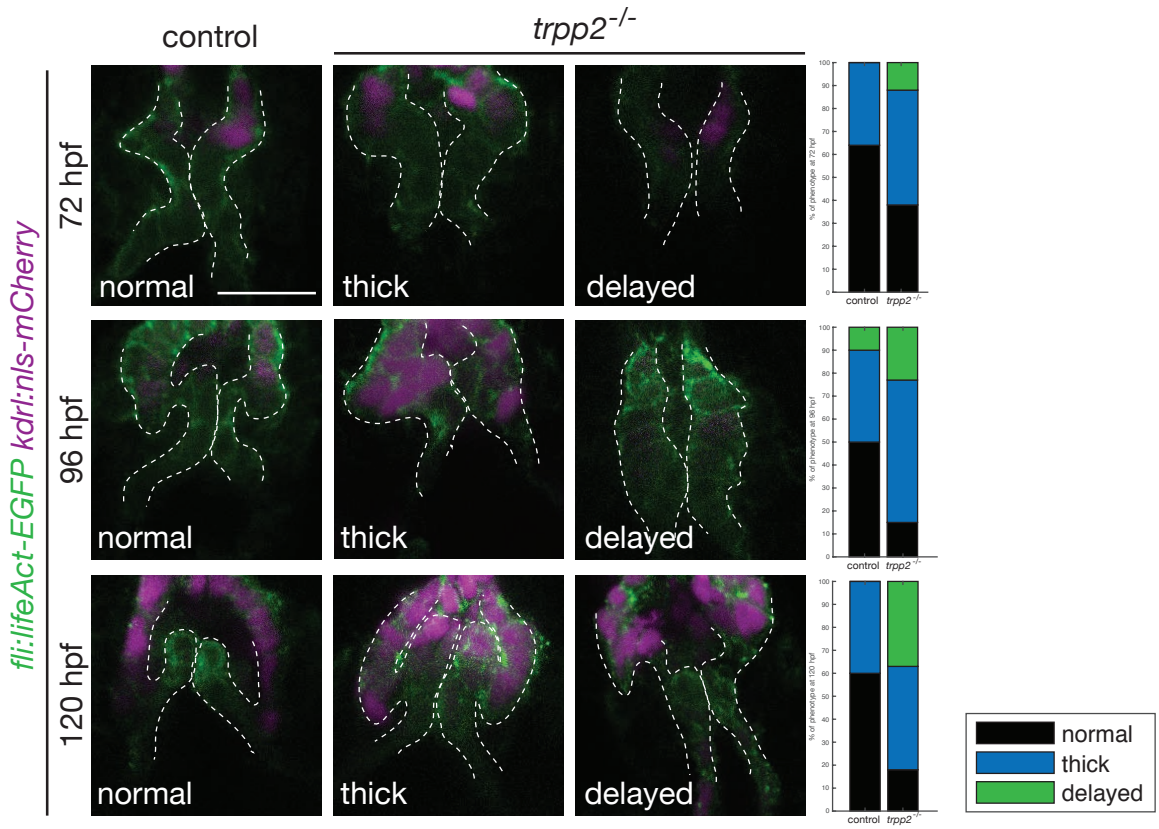


***Figure 8 – figure supplement 2 – Valve phenotypes in trpp2$^{-/-}$***

*Z-sections of the Tg(fli:lifeAct-EGFP: kdrl:nls-mCherry) in control (trpp2$^{+/+}$ and trpp$^{+/-}$) and trpp2$^{-/-}$ and quantifications of the phenotypes.*

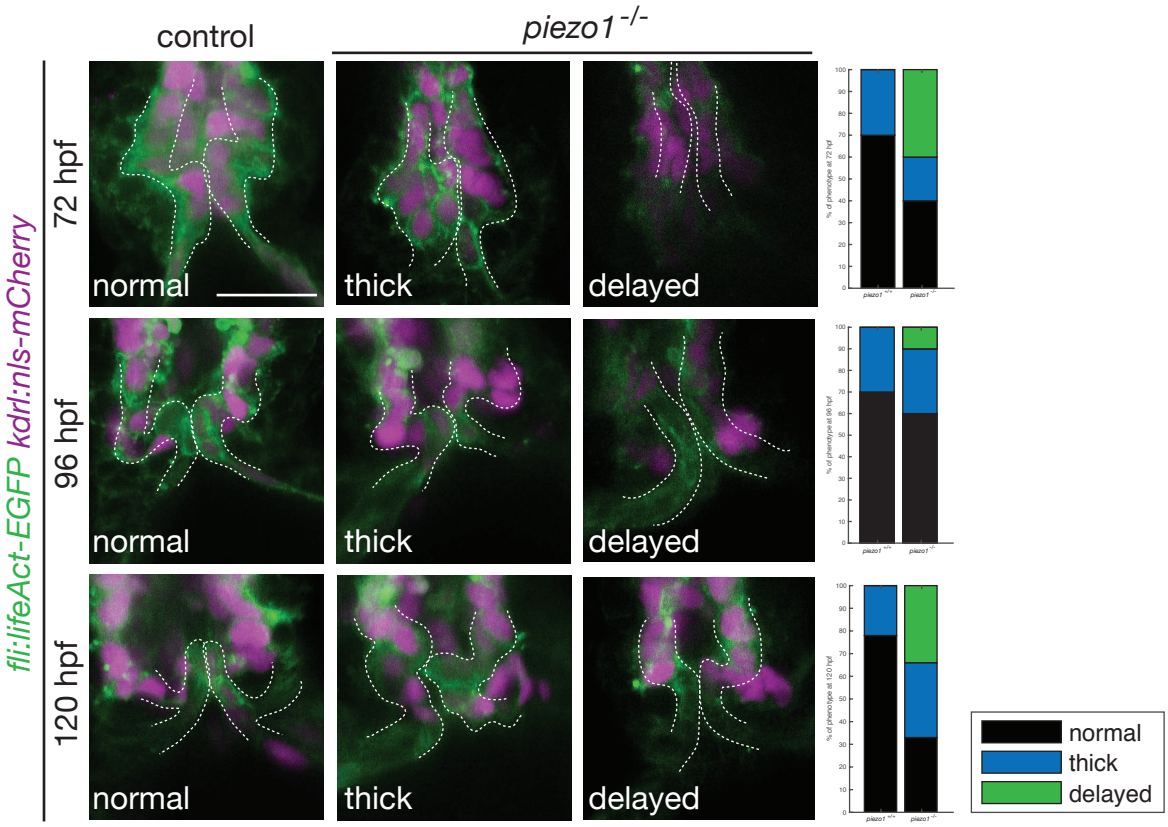


***Figure 8 – figure supplement 3 – Valve phenotypes in piezo1$^{-/-}$***

*Z-sections of the Tg(fli:lifeAct-EGFP: kdrl:nls-mCherry) in piezo1$^{+/+}$ and piezo1$^{-/-}$ and quantifications of the phenotypes.*

## Supplementary files

Figure8-Source Data File1. Excel file describing the independent experiments

**Acknowledgements**

We thank the Vermot laboratory for discussion and H. Fukui and R. Chow for thoughtful comments on the manuscript. We thank C. Burns and V. Lecaudey for providing antibodies and protocols for immunohistochemistry. We thank the IGBMC fish facility (S. Pajot and C. Moebs) and the IGBMC imaging center, in particular B. Gurchenkov, D. Hentsch, E. Guiot and E. Grandgirard. This study was supported by the European Research Council [682938 – EVALVE], Fondation pour la Recherche Médicale [DEQ29553], Agence Nationale de la Recherche [ANR-15-CE13-0015-01, ANR-10-IDEX-0002-02, ANR-12-ISV2-0001-01 and ANR-10-LABX-0030-INRT] and the European Molecular Biology Organization Young Investigator Program. H.V. was supported by the IGBMC International PhD program (ANR-10-LABX-0030-INRT). A.L.D. was supported by a post doctoral fellowship from the Lefoulon-Delalande Foundation.

**References**

Agarwala, S., Duquesne, S., Liu, K., Boehm, A., Grimm, L., Link, S., Konig, S., Eimer, S., Ronneberger, O., and Lecaudey, V. (2015). Amotl2a interacts with the Hippo effector Yap1 and the Wnt/beta-catenin effector Lef1 to control tissue size in zebrafish. Elife *4*, e08201.

Anton, H., Harlepp, S., Ramspacher, C., Wu, D., Monduc, F., Bhat, S., Liebling, M., Paoletti, C., Charvin, G., Freund, J.B.*, et al.* (2013). Pulse propagation by a capacitive mechanism drives embryonic blood flow. Development *140*, 4426-4434.

Back, M., Gasser, T.C., Michel, J.B., and Caligiuri, G. (2013). Biomechanical factors in the biology of aortic wall and aortic valve diseases. Cardiovasc Res *99*, 232-241.

Baeyens, N., Bandyopadhyay, C., Coon, B.G., Yun, S., and Schwartz, M.A. (2016). Endothelial fluid shear stress sensing in vascular health and disease. J Clin Invest *126*, 821-828.

Beis, D., Bartman, T., Jin, S.W., Scott, I.C., D'Amico, L.A., Ober, E.A., Verkade, H., Frantsve, J., Field, H.A., Wehman, A.*, et al.* (2005). Genetic and cellular analyses of zebrafish atrioventricular cushion and valve development. Development *132*, 4193-4204.

Boselli, F., Steed, E., Freund, J.B., and Vermot, J. (2017). Anisotropic shear stress patterns predict the orientation of convergent tissue movements in the embryonic heart. Development *144*, 4322-4327.

Braun, M.H., Brill, R.W., Gosline, J.M., and Jones, D.R. (2003a). Form and function of the bulbus arteriosus in yellowfin tuna (Thunnus albacares), bigeye tuna (Thunnus obesus) and blue marlin (Makaira nigricans): static properties. J Exp Biol *206*, 3311-3326.

Braun, M.H., Brill, R.W., Gosline, J.M., and Jones, D.R. (2003b). Form and function of the bulbus arteriosus in yellowfin tuna (Thunnus albacares): dynamic properties. J Exp Biol *206*, 3327-3335.

Butcher, J.T., Simmons, C.A., and Warnock, J.N. (2008). Mechanobiology of the aortic heart valve. J Heart Valve Dis *17*, 62-73.

Choi, D., Park, E., Jung, E., Seong, Y.J., Yoo, J., Lee, E., Hong, M., Lee, S., Ishida, H., Burford, J.*, et al.* (2017). Laminar flow downregulates Notch activity to promote lymphatic sprouting. J Clin Invest *127*, 1225-1240.

Combs, M.D. (2009). Circulation research *105*, 408-421.

Dina, C., Bouatia-Naji, N., Tucker, N., Delling, F.N., Toomer, K., Durst, R., Perrocheau, M., Fernandez-Friera, L., Solis, J., investigators, P.*, et al.* (2015). Genetic association analyses highlight biological pathways underlying mitral valve prolapse. Nat Genet *47*, 1206-1211.

Donat, S., Lourenco, M., Paolini, A., Otten, C., Renz, M., and Abdelilah-Seyfried, S. (2018). Heg1 and Ccm1/2 proteins control endocardial mechanosensitivity during zebrafish valvulogenesis. eLife *7*.

Durst, R., Sauls, K., Peal, D.S., deVlaming, A., Toomer, K., Leyne, M., Salani, M., Talkowski, M.E., Brand, H., Perrocheau, M.*, et al.* (2015). Mutations in DCHS1 cause mitral valve prolapse. Nature *525*, 109-113.

Dzamba, B.J., and DeSimone, D.W. (2018). Extracellular Matrix (ECM) and the Sculpting of Embryonic Tissues. Curr Top Dev Biol *130*, 245-274.

Eisenhoffer, G.T., Loftus, P.D., Yoshigi, M., Otsuna, H., Chien, C.B., Morcos, P.A., and Rosenblatt, J. (2012). Crowding induces live cell extrusion to maintain homeostatic cell numbers in epithelia. Nature *484*, 546-549.

L., Alqahtani A.M., MacGrogan D., Richardson R.V., Murphy L1, Salguero-Jimenez A., Sintes Rodriguez San Pedro M., Tiurma S1, McCutcheon L., Gilmore A1, de La Pompa JL., Chaudhry B., Henderson D.J. A novel source of arterial valve cells linked to bicuspid aortic valve without raphe in mice. Elife. 2018 Jun 29;7. pii: e34110.

Feaver, R.E., Gelfand, B.D., and Blackman, B.R. (2013). Human haemodynamic frequency harmonics regulate the inflammatory phenotype of vascular endothelial cells. Nat Commun *4*, 1525.

Garg, V. (2016). Notch Signaling in Aortic Valve Development and Disease. In Etiology and Morphogenesis of Congenital Heart Disease: From Gene Function and Cellular Interaction to Morphology, T. Nakanishi, R.R. Markwald, H.S. Baldwin, B.B. Keller, D. Srivastava, and H. Yamagishi, eds. (Tokyo), pp. 371-376.

Garg, V., Muth, A.N., Ransom, J.F., Schluterman, M.K., Barnes, R., King, I.N., Grossfeld, P.D., and Srivastava, D. (2005). Mutations in NOTCH1 cause aortic valve disease. Nature *437*, 270-274.

Godby, R.C., Munjal, C., Opoka, A.M., Smith, J.M., Yutzey, K.E., Narmoneva, D.A., and Hinton, R.B. (2014). Cross Talk between NOTCH Signaling and Biomechanics in Human Aortic Valve Disease Pathogenesis. J Cardiovasc Dev Dis *1*, 237-256.

Goddard, L.M., Duchemin, A.L., Ramalingan, H., Wu, B., Chen, M., Bamezai, S., Yang, J., Li, L., Morley, M.P., Wang, T.*, et al.* (2017). Hemodynamic Forces Sculpt Developing Heart Valves through a KLF2-WNT9B Paracrine Signaling Axis. Developmental cell *43*, 274-289 e275.

Hasan, S.S., Tsaryk, R., Lange, M., Wisniewski, L., Moore, J.C., Lawson, N.D., Wojciechowska, K., Schnittler, H., and Siekmann, A.F. (2017). Endothelial Notch signalling limits angiogenesis via control of artery formation. Nat Cell Biol *19*, 928-940.

He, L., Si, G., Huang, J., Samuel, A.D.T., and Perrimon, N. (2018). Mechanical regulation of stem-cell differentiation by the stretch-activated Piezo channel. Nature *555*, 103-106.

Heckel, E., Boselli, F., Roth, S., Krudewig, A., Belting, H.G., Charvin, G., and Vermot, J. (2015). Oscillatory Flow Modulates Mechanosensitive klf2a Expression through trpv4 and trpp2 during Heart Valve Development. Curr Biol *25*, 1354-1361.

Hoffman, J.I., and Kaplan, S. (2002). The incidence of congenital heart disease. J Am Coll Cardiol *39*, 1890-1900.

Jin, S.W., Beis, D., Mitchell, T., Chen, J.N., and Stainier, D.Y. (2005). Cellular and molecular analyses of vascular tube and lumen formation in zebrafish. Development *132*, 5199-5209.

Keith, D.A., Paz, A., Gallop, P.M., and Glimcher, M.J. (1977). Histologic and biochemical identification and characterization of an elastin in cartilage. J Histochem Cytochem *25*, 1154-1162.

Laforest, B., Andelfinger, G., and Nemer, M. (2011). Loss of Gata5 in mice leads to bicuspid aortic valve. J Clin Invest *121*, 2876-2887.

Lee, J.S., Yu, Q., Shin, J.T., Sebzda, E., Bertozzi, C., Chen, M., Mericko, P., Stadtfeld, M., Zhou, D., Cheng, L.*, et al.* (2006). Klf2 is an essential regulator of vascular hemodynamic forces in vivo. Dev Cell *11*, 845-857.

Lee, W., Leddy, H.A., Chen, Y., Lee, S.H., Zelenski, N.A., McNulty, A.L., Wu, J., Beicker, K.N., Coles, J., Zauscher, S.*, et al.* (2014). Synergy between Piezo1 and Piezo2 channels confers high-strain mechanosensitivity to articular cartilage. Proc Natl Acad Sci U S A *111*, E5114-5122.

Lewis, A.H., Cui, A.F., McDonald, M.F., and Grandl, J. (2017). Transduction of Repetitive Mechanical Stimuli by Piezo1 and Piezo2 Ion Channels. Cell Rep *19*, 2572-2585.

Li, J., Hou, B., Tumova, S., Muraki, K., Bruns, A., Ludlow, M.J., Sedo, A., Hyman, A.J., McKeown, L., Young, R.S.*, et al.* (2014). Piezo1 integration of vascular architecture with physiological force. Nature *515*, 279-282.

Lukacs, V., Mathur, J., Mao, R., Bayrak-Toydemir, P., Procter, M., Cahalan, S.M., Kim, H.J., Bandell, M., Longo, N., Day, R.W.*, et al.* (2015). Impaired PIEZO1 function in patients with a novel autosomal recessive congenital lymphatic dysplasia. Nat Commun *6*, 8329.

Luxan, G., D'Amato, G., MacGrogan, D., and de la Pompa, J.L. (2016). Endocardial Notch Signaling in Cardiac Development and Disease. Circ Res *118*, e1-e18.
Lyons, S.E., Lawson, N.D., Lei, L., Bennett, P.E., Weinstein, B.M., and Liu, P.P. (2002). A nonsense mutation in zebrafish gata1 causes the bloodless phenotype in vlad tepes. Proceedings of the National Academy of Sciences of the United States of America *99*, 5454-5459.
Ma, S., Cahalan, S., LaMonte, G., Grubaugh, N.D., Zeng, W., Murthy, S.E., Paytas, E., Gamini, R., Lukacs, V., Whitwam, T.*, et al.* (2018). Common PIEZO1 Allele in African Populations Causes RBC Dehydration and Attenuates Plasmodium Infection. Cell *173*, 443-455 e412.
MacGrogan, D., D'Amato, G., Travisano, S., Martinez-Poveda, B., Luxan, G., Del Monte-Nieto, G., Papoutsi, T., Sbroggio, M., Bou, V., Gomez-Del Arco, P.*, et al.* (2016). Sequential Ligand-Dependent Notch Signaling Activation Regulates Valve Primordium Formation and Morphogenesis. Circulation research *118*, 1480-1497.
Mack, J.J., Mosqueiro, T.S., Archer, B.J., Jones, W.M., Sunshine, H., Faas, G.C., Briot, A., Aragon, R.L., Su, T., Romay, M.C.*, et al.* (2017). NOTCH1 is a mechanosensor in adult arteries. Nat Commun *8*, 1620.
Miesfeld, J.B., and Link, B.A. (2014). Establishment of transgenic lines to monitor and manipulate Yap/Taz-Tead activity in zebrafish reveals both evolutionarily conserved and divergent functions of the Hippo pathway. Mech Dev *133*, 177-188.
Moriyama, Y., Ito, F., Takeda, H., Yano, T., Okabe, M., Kuraku, S., Keeley, F.W., and Koshiba-Takeuchi, K. (2016). Evolution of the fish heart by sub/neofunctionalization of an elastin gene. Nat Commun *7*, 10397.
Murthy, S.E., Dubin, A.E., and Patapoutian, A. (2017). Piezos thrive under pressure: mechanically activated ion channels in health and disease. Nat Rev Mol Cell Biol *18*, 771-783.
Nakajima, H., Yamamoto, K., Agarwala, S., Terai, K., Fukui, H., Fukuhara, S., Ando, K., Miyazaki, T., Yokota, Y., Schmelzer, E.*, et al.* (2017). Flow-Dependent Endothelial YAP Regulation Contributes to Vessel Maintenance. Dev Cell *40*, 523-536 e526.
Neto, F., Klaus-Bergmann, A., Ong, Y.T., Alt, S., Vion, A.C., Szymborska, A., Carvalho, J.R., Hollfinger, I., Bartels-Klein, E., Franco, C.A.*, et al.* (2018). YAP and TAZ regulate adherens junction dynamics and endothelial cell distribution during vascular development. Elife *7*.
Nicenboim, J., Malkinson, G., Lupo, T., Asaf, L., Sela, Y., Mayseless, O., Gibbs-Bar, L., Senderovich, N., Hashimshony, T., Shin, M.*, et al.* (2015). Lymphatic vessels arise from specialized angioblasts within a venous niche. Nature *522*, 56-61.
Ninov, N., Borius, M., and Stainier, D.Y. (2012). Different levels of Notch signaling regulate quiescence, renewal and differentiation in pancreatic endocrine progenitors. Development *139*, 1557-1567.
Nonomura, K., Lukacs, V., Sweet, D.T., Goddard, L.M., Kanie, A., Whitwam, T., Ranade, S.S., Fujimori, T., Kahn, M.L., and Patapoutian, A. (2018). Mechanically activated ion channel PIEZO1 is required for lymphatic valve formation. Proc Natl Acad Sci U S A.
Oyen, N., Poulsen, G., Boyd, H.A., Wohlfahrt, J., Jensen, P.K., and Melbye, M. (2009). Recurrence of congenital heart defects in families. Circulation *120*, 295-301.
Paffett-Lugassy, N., Novikov, N., Jeffrey, S., Abrial, M., Guner-Ataman, B., Sakthivel, S., Burns, C.E., and Burns, C.G. (2017). Unique developmental trajectories and genetic regulation of ventricular and outflow tract progenitors in the zebrafish second heart field. Development *144*, 4616-4624.
Pathak, M.M., Nourse, J.L., Tran, T., Hwe, J., Arulmoli, J., Le, D.T., Bernardis, E., Flanagan, L.A., and Tombola, F. (2014). Stretch-activated ion channel Piezo1 directs lineage choice in human neural stem cells. Proc Natl Acad Sci U S A *111*, 16148-16153.
Pestel, J., Ramadass, R., Gauvrit, S., Helker, C., Herzog, W., and Stainier, D.Y. (2016). Real-time 3D visualization of cellular rearrangements during cardiac valve formation. Development *143*, 2217-2227.

Phng, L.K., Stanchi, F., and Gerhardt, H. (2013). Filopodia are dispensable for endothelial tip cell guidance. Development *140*, 4031-4040.
Pitulescu, M.E., Schmidt, I., Giaimo, B.D., Antoine, T., Berkenfeld, F., Ferrante, F., Park, H., Ehling, M., Biljes, D., Rocha, S.F., *et al.* (2017). Dll4 and Notch signalling couples sprouting angiogenesis and artery formation. Nat Cell Biol *19*, 915-927.
Poole, K., Herget, R., Lapatsina, L., Ngo, H.D., and Lewin, G.R. (2014). Tuning Piezo ion channels to detect molecular-scale movements relevant for fine touch. Nat Commun *5*, 3520.
Qi, Y., Andolfi, L., Frattini, F., Mayer, F., Lazzarino, M., and Hu, J. (2015). Membrane stiffening by STOML3 facilitates mechanosensation in sensory neurons. Nat Commun *6*, 8512.
Ranade, S.S., Qiu, Z., Woo, S.H., Hur, S.S., Murthy, S.E., Cahalan, S.M., Xu, J., Mathur, J., Bandell, M., Coste, B., *et al.* (2014). Piezo1, a mechanically activated ion channel, is required for vascular development in mice. Proc Natl Acad Sci U S A *111*, 10347-10352.
Ranade, S.S., Syeda, R., and Patapoutian, A. (2015). Mechanically Activated Ion Channels. Neuron *87*, 1162-1179.
Retailleau, K., Duprat, F., Arhatte, M., Ranade, S.S., Peyronnet, R., Martins, J.R., Jodar, M., Moro, C., Offermanns, S., Feng, Y., *et al.* (2015). Piezo1 in Smooth Muscle Cells Is Involved in Hypertension-Dependent Arterial Remodeling. Cell Rep *13*, 1161-1171.
Richards, A.A., and Garg, V. (2010). Genetics of congenital heart disease. Curr Cardiol Rev *6*, 91-97.
Sabine, A., Agalarov, Y., Maby-El Hajjami, H., Jaquet, M., Hagerling, R., Pollmann, C., Bebber, D., Pfenniger, A., Miura, N., Dormond, O., *et al.* (2012). Mechanotransduction, PROX1, and FOXC2 cooperate to control connexin37 and calcineurin during lymphatic-valve formation. Dev Cell *22*, 430-445.
Sabine, A., Bovay, E., Demir, C.S., Kimura, W., Jaquet, M., Agalarov, Y., Zangger, N., Scallan, J.P., Graber, W., Gulpinar, E., *et al.* (2015). FOXC2 and fluid shear stress stabilize postnatal lymphatic vasculature. J Clin Invest *125*, 3861-3877.
Samsa, L.A., Givens, C., Tzima, E., Stainier, D.Y., Qian, L., and Liu, J. (2015). Cardiac contraction activates endocardial Notch signaling to modulate chamber maturation in zebrafish. Development *142*, 4080-4091.
Sanchez-Iranzo, H., Galardi-Castilla, M., Minguillon, C., Sanz-Morejon, A., Gonzalez-Rosa, J.M., Felker, A., Ernst, A., Guzman-Martinez, G., Mosimann, C., and Mercader, N. (2018). Tbx5a lineage tracing shows cardiomyocyte plasticity during zebrafish heart regeneration. Nat Commun *9*, 428.
Sauls, K., de Vlaming, A., Harris, B.S., Williams, K., Wessels, A., Levine, R.A., Slaugenhaupt, S.A., Goodwin, R.L., Pavone, L.M., Merot, J., *et al.* (2012). Developmental basis for filamin-A-associated myxomatous mitral valve disease. Cardiovasc Res *96*, 109-119.
Scherz, P.J., Huisken, J., Sahai-Hernandez, P., and Stainier, D.Y. (2008). High-speed imaging of developing heart valves reveals interplay of morphogenesis and function. Development *135*, 1179-1187.
Schottenfeld, J., Sullivan-Brown, J., and Burdine, R.D. (2007). Zebrafish curly up encodes a Pkd2 ortholog that restricts left-side-specific expression of southpaw. Development *134*, 1605-1615.
Sehnert, A.J., Huq, A., Weinstein, B.M., Walker, C., Fishman, M., and Stainier, D.Y. (2002). Cardiac troponin T is essential in sarcomere assembly and cardiac contractility. Nat Genet *31*, 106-110.
Steed, E., Boselli, F., and Vermot, J. (2016a). Hemodynamics driven cardiac valve morphogenesis. Biochim Biophys Acta *1863*, 1760-1766.
Steed, E., Faggianelli, N., Roth, S., Ramspacher, C., Concordet, J.P., and Vermot, J. (2016b). klf2a couples mechanotransduction and zebrafish valve morphogenesis through fibronectin synthesis. Nat Commun *7*, 11646.

Stefanovic, S., Barnett, P., van Duijvenboden, K., Weber, D., Gessler, M., and Christoffels, V.M. (2014). GATA-dependent regulatory switches establish atrioventricular canal specificity during heart development. Nat Commun *5*, 3680.

Sweet, D.T., Jimenez, J.M., Chang, J., Hess, P.R., Mericko-Ishizuka, P., Fu, J., Xia, L., Davies, P.F., and Kahn, M.L. (2015). Lymph flow regulates collecting lymphatic vessel maturation in vivo. J Clin Invest *125*, 2995-3007.

Tammela, T., Zarkada, G., Nurmi, H., Jakobsson, L., Heinolainen, K., Tvorogov, D., Zheng, W., Franco, C.A., Murtomaki, A., Aranda, E.*, et al.* (2011). VEGFR-3 controls tip to stalk conversion at vessel fusion sites by reinforcing Notch signalling. Nat Cell Biol *13*, 1202-1213.

Vermot, J., Forouhar, A.S., Liebling, M., Wu, D., Plummer, D., Gharib, M., and Fraser, S.E. (2009). Reversing blood flows act through klf2a to ensure normal valvulogenesis in the developing heart. PLoS biology *7*, e1000246.

Wang, Y., Wu, B., Farrar, E., Lui, W., Lu, P., Zhang, D., Alfieri, C.M., Mao, K., Chu, M., Yang, D.*, et al.* (2017). Notch-Tnf signalling is required for development and homeostasis of arterial valves. Eur Heart J *38*, 675-686.

Wu, B., Wang, Y., Xiao, F., Butcher, J.T., Yutzey, K.E., and Zhou, B. (2017). Developmental Mechanisms of Aortic Valve Malformation and Disease. Annu Rev Physiol *79*, 21-41.

Zarychanski, R., Schulz, V.P., Houston, B.L., Maksimova, Y., Houston, D.S., Smith, B., Rinehart, J., and Gallagher, P.G. (2012). Mutations in the mechanotransduction protein PIEZO1 are associated with hereditary xerocytosis. Blood *120*, 1908-1915.